NASA/TM—20240011830

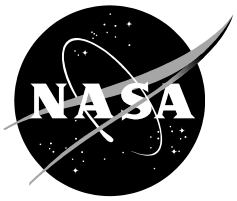

Evaluation of Aluminum Polymer Capacitors for Space Applications

Alexander A. Teverovsky

October 2024

NASA STI Program Report Series

The NASA STI Program collects, organizes, provides for archiving, and disseminates NASA's STI. The NASA STI program provides access to the NTRS Registered and its public interface, the NASA Technical Reports Server, thus providing one of the largest collections of aeronautical and space science STI in the world. Results are published in both non-NASA channels and by NASA in the NASA STI Report Series, which includes the following report types:

- TECHNICAL PUBLICATION. Reports of completed research or a major significant phase of research that present the results of NASA Programs and include extensive data or theoretical analysis. Includes compilations of significant scientific and technical data and information deemed to be of continuing reference value. NASA counterpart of peer-reviewed formal professional papers but has less stringent limitations on manuscript length and extent of graphic presentations.

- TECHNICAL MEMORANDUM. Scientific and technical findings that are preliminary or of specialized interest, e.g., quick release reports, working papers, and bibliographies that contain minimal annotation. Does not contain extensive analysis.

- CONTRACTOR REPORT. Scientific and technical findings by NASA-sponsored contractors and grantees.

- CONFERENCE PUBLICATION. Collected papers from scientific and technical conferences, symposia, seminars, or other meetings sponsored or co-sponsored by NASA.

- SPECIAL PUBLICATION. Scientific, technical, or historical information from NASA programs, projects, and missions, often concerned with subjects having substantial public interest.

- TECHNICAL TRANSLATION. English-language translations of foreign scientific and technical material pertinent to NASA's mission.

Specialized services also include organizing and publishing research results, distributing specialized research announcements and feeds, providing information desk and personal search support, and enabling data exchange services.

For more information about the NASA STI program, see the following:

- Access the NASA STI program home page at http://www.sti.nasa.gov

- Help desk contact information:

https://www.sti.nasa.gov/sti-contact-form/ and select the "General" help request type.

NASA/TM—20240011830

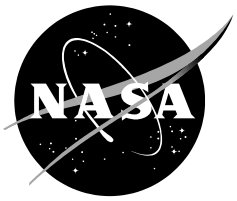

Evaluation of Aluminum Polymer Capacitors for Space Applications

Alexander A. Teverovsky
Jacobs Engineering Group, Lanham MD

National Aeronautics and
Space Administration

Goddard Space Flight Center
Greenbelt, MD 20771

October 2024

Acknowledgments (optional)

This work was sponsored by the NASA Electronic Parts and Packaging (NEPP) Program.

Available from

NASA STI Program
Mail Stop 148
NASA's Langley Research Center
Hampton, VA 23681-2199

National Technical Information Service
5285 Port Royal Road
Springfield, VA 22161
703-605-6000

This report is available in electronic form at

https://nepp.nasa.gov/

Stress Testing of Chip Aluminum Polymer Capacitors

Abstract

Layered aluminum polymer capacitors (APC) may be viable replacements to currently used chip tantalum capacitors due to their lower ESR, weight, and smaller size. So far, there is a lack of information regarding the reliability of these parts. Available technical literature is mostly related to the effect of humidity. Although APCs have a limited moisture resistance, it may be contained to the level sufficient for space applications. This work analyzes construction and characteristics of seven types of commercial APCs manufactured by four vendors and rated to voltages from 6.3 to 35 V were analyzed. Their reliability under environmental stresses and highly accelerated life tests was assessed in the range of temperatures and voltages to determine reliability acceleration factors. For this purpose, characteristics of the parts, including breakdown voltages, the level of anomalous charging currents (ACC), capacitance, DF, ESR and leakage currents were measured in the process of storage at high-temperatures (from 100 to 150 °C) and high humidity at 85 °C. Monitored highly accelerated life tests have been carried out at temperatures of 85 °C and 125 °C and voltages varying from 1.2 to 1.9 times the rated voltage. Degradation processes and reliability of APCs have been compared to polymer tantalum capacitors.

Contents

Stress Testing of Chip Aluminum Polymer Capacitors 2
Abstract 2
I. Introduction 2
II. Experiment 4
III. High temperature storage 4
IV. Effect of humidity 6
V. Highly accelerated life testing 9
VI. Summary 14
VII. Acknowledgment 15
VIII. References 15
Appendix A. Characteristics of Aluminum Polymer Capacitors 17
Analysis of data sheets 17
Storage conditions 18
Qualification testing 18
Experimental data 19
AC characteristics 19
Leakage currents 20
Breakdown voltages 22
Effect of reverse bias 25
Appendix B. Construction Analysis of Aluminum Polymer Capacitors 26

I. Introduction

Aluminum electrolytic capacitors with conductive polymer cathodes appeared on the market at the turn of this century, first in cylinder aluminum cases that employed wound sheets of oxidized aluminum foil. The design of these parts was similar to wet electrolytic capacitors that also used anodized rolled aluminum foils. A replacement of wet electrolyte with conductive polymers allowed for a substantial reduction of the equivalent series resistance (ESR) and eliminated one of its most significant reliability problem – evaporation of electrolyte. Chip aluminum polymer

capacitors (APC) with stacked oxidized aluminum plates encapsulated in molded cases and capable for surface mount assembly were introduced by KEMET and CDE in 2001 [1, 2]. Currently (2023), Murata manufactures 21 types of ECAS series of APCs in case size 7343 and thickness from 1.4 to 2.8 mm. Parts have capacitances from 15 to 470 μF, voltage ratings from 2 to 25 V, and ESR from 4.5 to 40 mohm. The parts have operating temperature range from -40 °C to 105 °C [3].

Presently, most APCs are manufactured in cylinder cases, but there is an increasing production trend of chip designs by Kemet, CDE, Panasonic, Murata, Wurth Elektronik, AVX, and others. Chips are typically rated to low voltages, below 35 V, with the largest group (~71%) rated between 2 and 4 V, and only ~4% are rated between 20 and 35 V. However, development of new conductive PEDOT:PSS polymers with special additives allows for a substantial increase of operating voltages up to 450 V [4, 5].

The majority of APCs compliant with AEC-Q200 requirements have cylinder case designs and there are only a few types of capacitors produced for automotive industry. Although most chip APCs are manufactured for general purposes and have an operating temperature range from -55 to +105 °C, some types of capacitors are rated to 135 °C [6]. Recently, KEMET introduced A798 series of APCs capable to operate at 125 °C for 3000 hours and withstand 85 °C, 85% RH at rated voltages for 1000 hours [7]. Newly developed Clevios K conductive polymer dispersion in aluminum radial capacitors allowed for achieving lifetimes over 1000 hours at 150 °C [8].

The expected lifetime of liquid aluminum electrolytic capacitors is assumed to double when temperature is reduced by 10 °C, $L \sim 2^{\Delta T/10}$, which corresponds to an activation energy of ~ 0.68 eV. According to Wurth Elektronik, the life of chip APCs increases tenfold when the temperature is reduced by 20 °C, $L \sim 10^{\Delta T/20}$ [9]. This corresponds to a much higher activation energy of ~1.7 eV. At these conditions, 2000 hours life testing at 125 °C would be equivalent to 228 years at operating temperature of 65 °C.

Based on Panasonic reliability test results, the failure rate for SP- series of capacitors is below 8.2 FIT at 105 °C and rated voltage. However, the estimated market failure rate is less than 0.13 FIT at a confidence level of 60% [10]. Leakage currents of APCs may increase after reflow soldering, under no-load conditions at high temperatures, or in high temperature and high humidity environments. However, in most cases, SP capacitors reduce leakage currents due to self-recovery actions when voltage is applied.

The failure rate for ECAS type APCs manufactured by Murata estimated from the results of returned failed products (customer's incoming inspection, in-process, field failures, etc.) is below 0.5 FIT [3]. The expected lifetime is calculated by the power law, $L \sim 2^{\Delta T/\theta}$; however, parameters of this equation are not disclosed because they vary depending on the type of product.

According to CDE [2], the wear-out (WO) mechanism of APCs' failure is due to a steady increase of ESR caused by the presence of moisture entrapped at the oxide/conductive polymer interface during manufacturing. The sensitivity to moisture was reduced substantially with a new design of ESRH capacitors that can operate at 125 °C and have expected life of more than 10 years in typical, hot running, DC-DC modules. The expected life equation is presented in a form: $L = A \times exp\left[\frac{E_a}{k}\left(\frac{1}{T} - 0.00279\right)\right] \times exp\left[C\left(\frac{1}{RH} - \frac{1}{90}\right)\right]$, where A = 1606 hr, E_a = 0.94 eV, C = 550, T is the temperature in K, and RH is the relative humidity in %.

Reliability of plastic encapsulated APCs with PEDOT conductive polymers in humid environments was studied by CALCE researchers at UMD [11, 12]. The observed dominant failure modes were an increase of leakage current, decrease of capacitance, and increase of ESR. The leakage current failures were due to iron particles in the dielectric aluminum oxide layer that provided paths for the current leakage. The iron particles originated from the iron salt used in the manufacturing process during cathode formation. Based on results of testing at rated voltages in humidity chambers at 85% RH and temperatures of 85 °C and 110 °C, the activation energy of failures caused by capacitance degradation was ~ 0.43 eV. The characteristic life time during testing at high humidity differs more than three times (from 550 to 1190 hours) for capacitors from different manufacturers.

Initial characterization of APCs by the NASA Electronic Parts and Packaging (NEPP) program was carried out by D. Liu in 2009 [13] using capacitors manufactured by 5 vendors and rated from 2 to 12 V. All parts had a footprint of EIA 7343. Results of testing showed that 12 thermal vacuum cycles at 10^{-4} Torr between -44 and +105 °C did not

significantly change the parts' characteristics. Chip capacitors with laminated structure exhibited the best performance by having lower ESR and higher breakdown voltages compared to cylinder case capacitors with rolled foil.

Considering the progress in design and materials used in manufacturing of chip APCs and the lack of reliability data, there is a need for the performance evaluation of capacitors under stress conditions similar to the quality assessments used for polymer tantalum capacitors (PTC) intended for space applications [14]. In this work, seven types of APCs from four vendors were tested in the process of long-term storage at high temperatures, high humidity, and operation at high temperatures and voltages (monitored highly accelerated life testing, HALT). Degradation processes and acceleration factors for environmental stresses and HALT are discussed and compared to the data for PTCs.

II.Experiment

Data sheet characteristics of APCs used in this study are shown in Table II.1. The parts were manufactured by four vendors with the same footprint, 7.3×4.3 mm, and thickness of the case (*H*) that varied from 1.9 to 2.8 mm.

Table II.1. Specified characteristics of the parts used in this study.

Group	Mfr.	C, µF	VR, V	ESR, mohm	DF, %	DCL, µA	T_max, °C	H, mm
1	A	120	6.3	9	6	75	105	1.9
2	B	180	6.3	10	6	45	125	2.8
3	C	150	6.3	15	6	94.5	105	1.9
4	D	100	6.3	15	6	63	105	1.9
5	B	33	10	18	6	13	125	2
6	B	15	25	40	6	15	125	2
7	B	15	35	40	6	53	125	2.8

Capacitance and dissipation factor (DF) were measured at 120 Hz, and ESR at 100 kHz. Different manufacturers are specifying measurements of DC leakage currents (DCL) after 2 to 5 min of electrification. In this work, leakage currents were monitored over time and to reduce the effect of absorption currents, DCL measurements were taken after 1000 sec of electrification. These conditions characterize better operational leakage currents that are typically at least two orders of magnitude below the specified values. Breakdown voltages (VBR) were measured similar to tantalum polymer capacitors by using a constant currents stress (CCS) test [15], and the level of anomalous charging currents (ACC) was characterized using the power surge testing method [16].

III.High temperature storage

High temperature storage (HTS) was carried out in temperature chambers set to 100, 125, and 150 °C using 5 samples for each temperature condition. All part types shown in Table II.1 have been tested for up to 4000 hours, and examples of degradation of AC characteristics in the process of storage for two types of capacitors (180 µF, 6.3 V and 15 µF, 35 V) are shown in Fig. III.1. The rate of degradation increased substantially with temperature and although none of the parts could endure 1000 hours at 150 °C, degradation in all groups was within the acceptable limits after 1000 hours at 125 °C and 6 out of 7 groups passed 4000 hours at 100 °C.

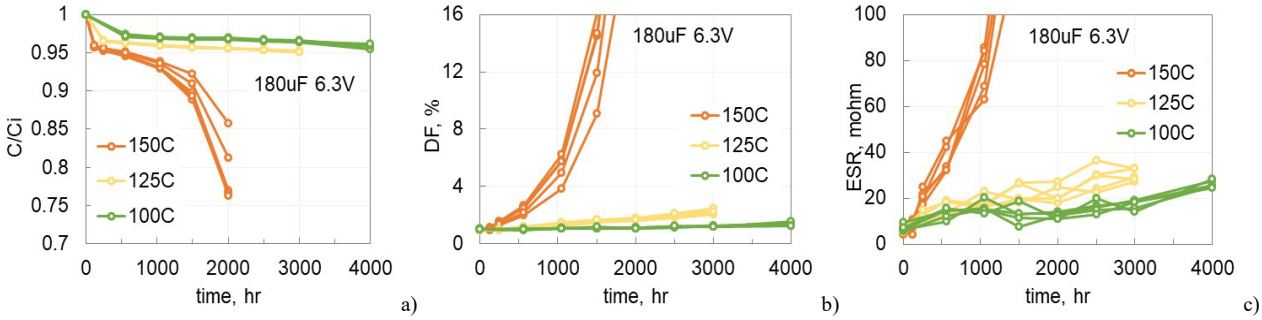

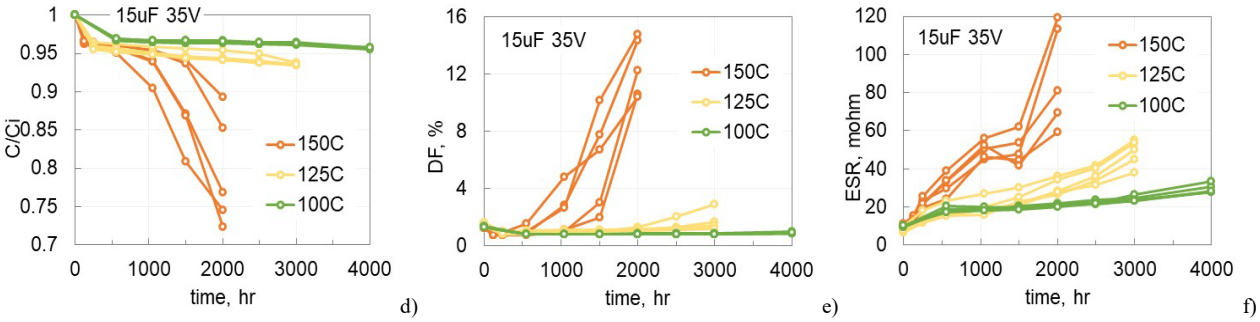

Fig. III.1. Variations of normalized capacitance (a, d), DF (b, e) and ESR (c, f) for 180 µF 6.3 V (a - c) and 15 µF 35 V (d - f) during HTS at three temperatures.

The parts are considered parametric failures if their capacitance decreased more than 10% of the initial value, or if DF increased more than 2 times of the initial limit (IL), or if ESR increased more than 3 times of the IL. The times to failure (TTF) were determined for each sample either directly from the curves similar to Fig.III.1 or by extrapolation of the data as shown in Fig.III.2a. Median times to failure calculated based on TTF distributions for capacitances and ESR are plotted in Arrhenius coordinates in Fig. III.2.b and c. Activation energies of the degradation varied from 0.64 to 0.9 eV for capacitance and in somewhat wider range, from 0.57 to 1.03 eV for ESR failures. However, the average activation energies were practically the same, $E_{a\_C} = 0.73 \pm 0.1$ eV, and $E_{a\_ESR} = 0.73 \pm 0.16$ eV. Extrapolation of the lines in Fig. III.2 to 65 °C that is assumed as the temperature of applications, resulted in the median TTF values from 6 to 48 years.

The values of E_a for PTCs were similar and also varied in a wide range, from 0.38 to 0.93 eV, averaging at 0.62 ±0.17 eV [17]. For both types of capacitors, the degradation was due to thermo-oxidative processes in conductive polymers and should be substantially less in vacuum compared to air environments. For this reason, successful results of qualification testing at 125 ºC for 1000 hours in air should guarantee long-term stability of characteristics at operating conditions in vacuum.

Another possible reason for APCs degradation during HTS is increasing of ESR due to changes in the hydrated layer of the Al2O3 dielectric. According to [2], water molecules trapped at the interfaces between the conductive polymer and oxide during manufacturing can form aluminum hydroxide that is conductive and might acts as an additional resistive layer in series with the conductive polymer. However, our data show that contrary to PTCs, where the rate of degradation of ESR is substantially greater than degradation of capacitance, the values of TTF_C and TTF_{ESR} for APCs are similar (see Fig. III.2 b, c). It is possible that the difference is due to a diffusion delay associated with penetration of oxygen inside the deep and narrow pores of aluminum oxide filled with conductive polymer compared to the sponge-like structure of the pores covered with a relatively thin layer of conductive polymer in tantalum capacitors. This structure of pores in PTCs enhances diffusion processes and results in a faster degradation of ESR.

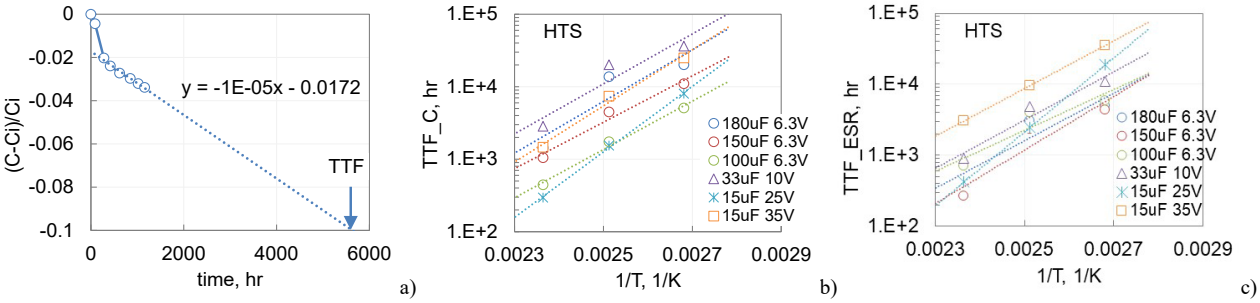

Fig. III.2. TTF calculation (a) and temperature dependencies of median times to parametric capacitance failures determined as a decrease by 10% compared to the initial value (b) and ESR failures (c) determined as a 3-time increase compared to the specified value.

HTS resulted in a substantial, up to three orders of magnitude, increase in currents after HTS at 150 °C for all part types (see Fig. III.3.a, b). At 125 °C, the increase was also noticeable, up to an order of magnitude, but storage at 100 °C for 4000 hours did not change currents significantly. The charts in Fig. III.3 also show variations of leakage currents after simulations by three reflow cycles at T_{max} = 235 °C for 4 types of APCs rated to 6.3 V. Due to a short duration of exposure to high temperatures, solder reflow did not cause significant variations in leakage currents.

A noticeable increase of DCL, up to two orders of magnitude, in wet tantalum and aluminum electrolytic capacitors after HTS was reported earlier [18]. It is possible that one of the reasons for DCL degradation in APCs is also due to the release of trapped electrons from deep states inside of Al2O3 dielectric that reduces the barrier at the interface oxide/conductive polymer and increases the Schottky conductivity through the dielectric. Another possible mechanism of increasing leakage currents is dissociation and out-diffusion of water molecules from the outer, hydrated layer of the aluminum oxide that can cause embrittlement of the layer and an increase in concentration of defects [19]. A substantial, about three orders of magnitude, increase in leakage currents after 2000 hours at 150 °C might be also due to mechanical damage in the deep pores in aluminum foil filled with polymer having a much larger coefficient of thermal expansion (CTE) compared to aluminum and Al2O3.

Breakdown voltages decreased after HTS for all part types except for 150 µF 6.3 V and 15 µF 25 V. Three cycles of reflow soldering resulted in approximately 10% reduction of breakdown voltages. Anomalous charging currents, ACC, were not detected in any of the parts before or after HTS. As it will be shown in the next section, the presence of moisture increases breakdown voltages. Respectively, desorption of water molecules during HTS decreased VBR.

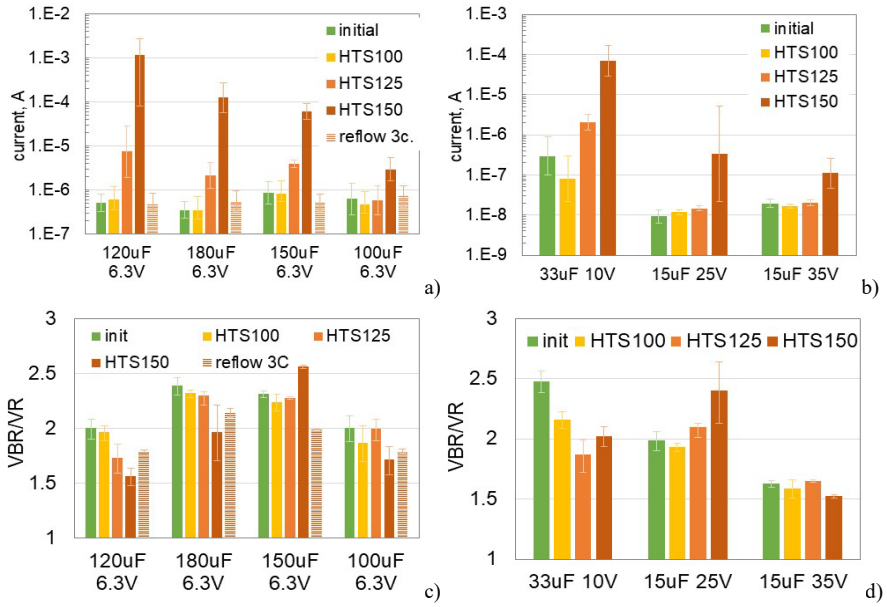

Fig. III.3. Effect of HTS on median values of DCL (a, b) and average values of breakdown voltages (c, d) for the seven types of APCs. Note that here and below, error bars indicate standard deviation of the relevant distributions.

IV.Effect of humidity

The effect of storage in humid environments was evaluated at three conditions: (1) 20 °C, 95% RH for 1500 hr, (2) 85 °C, 60% RH for 500 hr, and (3) 85 °C, 85% RH for 850 hr. AC characteristics were measured periodically through the testing using five samples from each part type. Measurements of leakage currents and breakdown voltages were carried out after humidity testing.

Results of measurements of AC characteristics for capacitors from groups 5, 6, and 7 (refer to Table II.1) during storage at 20 °C and 95% RH are shown in Fig. IV.1. Most variations of capacitance and DF occur by 1000 hours of storage; but after, characteristics continued changing, but at a lower rate. The increase of capacitance after 1500 hours was ~ 5% for gr.5 and gr.7 and 17% for gr.6. Dissipation factors increased by a factor of 2-3 times, but remained within the specified limits. The most surprizing result of these tests was the stability and limited change in ESR (variations below 30%).

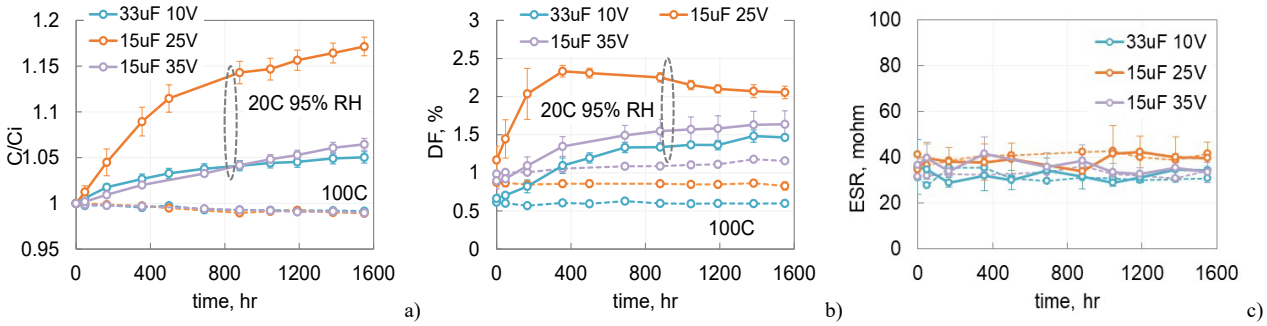

Fig. IV.1. Variations of normalized to the initial value capacitance (a), DF (b) and ESR (c) with time of storage at 20 °C and 95% RH (solid lines). As a reference, dashed lines show variations of characteristics during HTS at 100 °C (HTS100).

Measurements during storage at 85 °C and 60% RH (see Fig. IV.2) show that the increase of capacitance stabilizes by less than 200 hours at the levels that are 3% to 6% higher than the initial values. An increase in DF was less than 2.5 times, and most of the parts, had stable ESR values, except for gr.3 where ESR have risen by approximately 50%.

For most part types, variations of capacitance in the process of storage at 85 °C and 85% RH (see Fig. IV.3) stabilized also by 200 hours, but for gr.2 and especially for gr.3, capacitance did not stabilize even after 850 hours. By the end of the testing, the increase of capacitance varied from 5% in groups 1 and 4, and to 35% in gr.3. Dissipation factors had a tendency of gradual increasing for all part types, but the increase was especially notiecable for gr.3 where DF at the end of testing exceeded the specified limit of 6% more than two times. The values of ESR remained stable for all parts, except for gr.3, where degradation started after 400 hours of storage, and by the end of the testing exceeded the specified limit more than ten times.

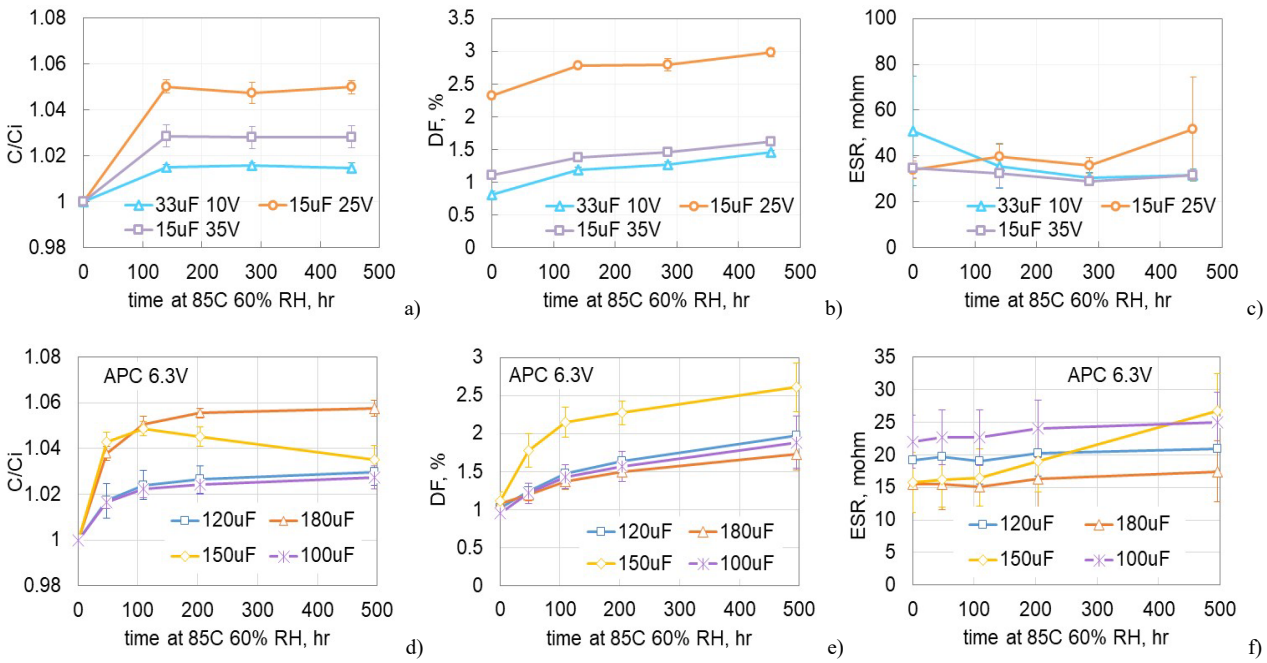

Fig. IV.2. Variations of normalized capacitance (a, d), DF (b, e) and ESR (c, f) with time of storage at 85 °C and 60% RH for capacitors rated to 10 V and above (a-c) and for 6.3 V capacitors (d-f).

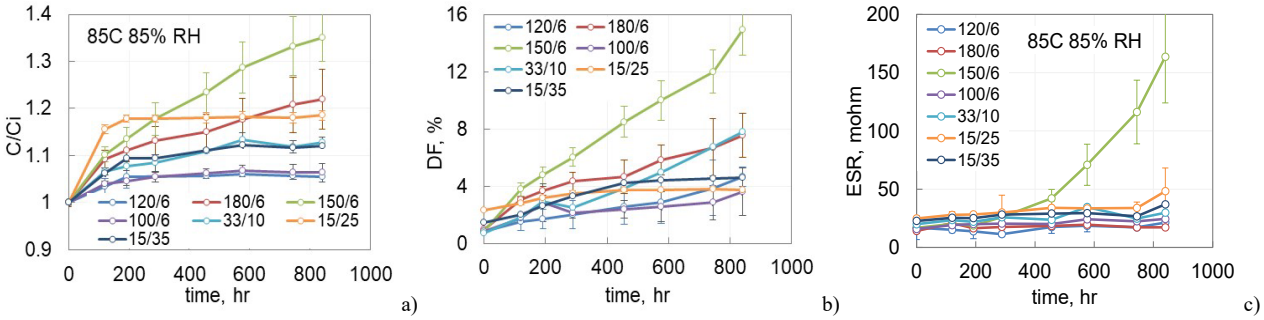

Fig. IV.3. AC characteristics for the seven types of capacitors in the process of storage at 85 °C and 85% RH. The legends indicate values of capacitors in μF and rated voltages in volts.

Variations of capacitance for APCs were similar to what was observed for PTCs [20] but degradation of DF was larger, likely due to the presence of the outer hydrated oxide layer in aluminum electrolytic capacitors. This layer can be easily polarized and generate relatively large losses [19]. Apparently, additional hydration caused by exposure to high temperature and high humidity can result in degraded DF values.

Results of post humidity storage measurements of operational leakage currents (currents measured after 1000 sec of electrificationa) and breakdown voltages normalized to the rated voltage are shown in Fig. IV.4. For comparison, breakdown voltages measured for dry capacitors (after 100 hours of HTS100) and capacitors after long (more than 3 month) storage at room conditions (RC) are also shown.

For all part types, except for gr.1 and gr.4, leakage currents increased approximately two orders of magnitude after storage at 85 °C and 85% RH. Note, that these two groups had no significant changes in leakage currents after storage at 60% RH and had also more stable AC characteristics. All parts after storage at 85 °C and 60% RH had leakage currents within the specified limits. Degradation of AC and DC characteristics caused by moisture sorption apparently does not depends on the thickness of the plastic packages. The rate and degree of degradation for gr.2 and gr.7 that had $H = 2.8$ mm was not less than for the rest of the parts having $H = 1.9$ mm.

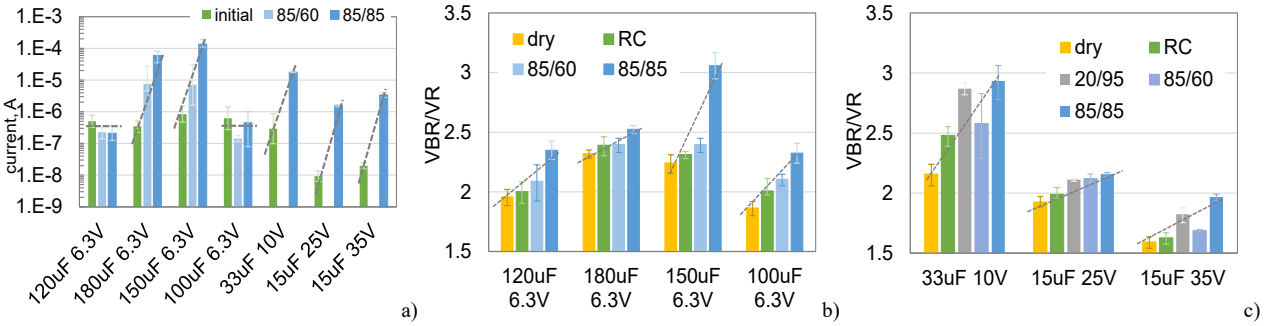

Fig. IV.4. Effect of storage in humidity chambers on median values of leakage currents (a) and average values of the normalized breakdown voltages (b, c).

The behavior of leakage currents in APCs was different from TPCs, where currents reduced in the presence of moisture due to the suppression of anomalous transients and remained stable up to 1000 hours of storage at 85 °C 85% RH. However, the effect of moisture on breakdown voltages was similar. The presence of moisture increased VBR in different APCs by 10 to 36% (see Fig.IV.4.b and c). On average, the increase of VBR after storage at 85 °C and 85% RH was 23 ±10%. This is similar to what was observed in PTCs [21] where breakdown voltages for 14 lots of capacitors increased by 21 ±14%. For PTCs this effect was explained by reduction of leakage currents, but for APCs that did not have anomalous transients, the prevailing mechanism is different. For APCs the effect is likely due to additional anodic oxidation of the defective areas in the dielectric in the presence of moisture and high electric fields that results in effective self-healing of the parts before breakdown.

Relaxation of leakage currents in capacitors rated to 6.3 V measured initially, after storage at 85 °C and 85% RH and after 1000-hour testing at 20 °C and 9 V are shown in Fig. IV.5. After saturation with moisture, leakage currents in gr.2 and gr.3 capacitors increased substantially (~ two orders of magnitude), but decreaed with time under bias. This

decrease is especially noticeable during 1000 hr testing at 9 V. After approximately an hour, currents in these groups started decreasing gradually, roughly inversely proportional with time, and by 1000 hours reduced to almost three orders of magnitude. The post stress leakage currents at 6.3 V were about an order of magnitude smaller than initially (compare Fig. IV.5.a and d).

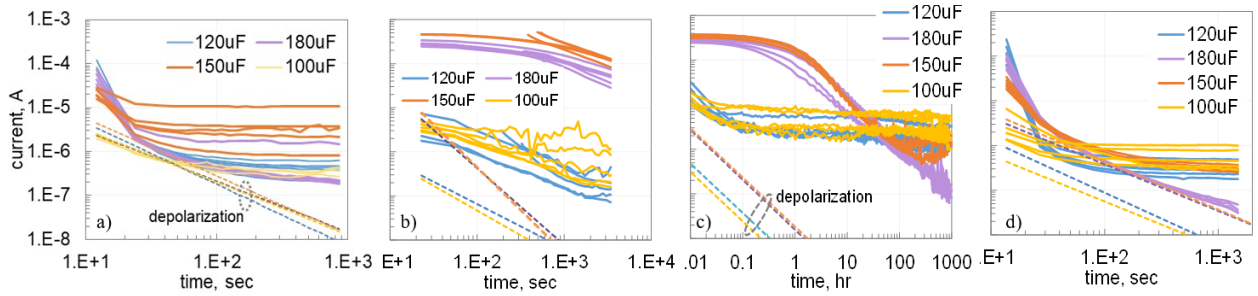

Fig. IV.5. Leakage currents in APCs rated to 6.3 V initially (a), after humidity chamber at 85 °C 85% RH for 850 hr (b), during post-humidity 1000-hour stress test at 9 V (c), and after stress testing (d). Dashed lines correspond to absorption currents in the parts measured during tepolarization.

Additional tests showed that the moisture diffusion delay in the parts at room conditions is more than 10 hours, and noticeable changes caused by moisture desorption start after ~ 30 hours. This means that the observed decrease in leakage currents can not be explained by moisture outdiffusion only. It is possible that additional anodic oxidation in the presence of moisture self-healed defects in the oxide and reduced leakage currents. Another possible mechanism is electron trapping in deep states of the oxide or in conductive polymer that increased the Schottky barrier and reduced conduction in the capacitors. Apparently, manufacturing conditions during oxide and conductive polymer formations in groups 2 and 3 capacitors were different compared to groups 1 and 4. This is also confirmed by variation of absorption (depolarization) currents. Initially, these currents were similar in all four types of capacitors; however, after storage in humidity chamber, absorption currents for groups 2 and 3 were almost an order of magnitude greater indicating an increased concentration of traps in these parts [20]. It is also possible that the presence of moisture intensifies processes of uptake and release of ionic charges in the bulk of conductive polymers that contribute to the absorption capacitance and currents in the system [22].

V.Highly accelerated life testing

HALT for capacitors rated to 6.3 V was carried out using 20 smaples in each group. All parts were reflow soldered onto test boards and each capacitor was connected in series with a 62 mA fast acting fuse. Voltage drops across the fuses were monitored by scanning voltages across the fuses that had 7 ohm resistance alowing for assessments of the leakage currents and determining times of failure by open fuses. First, the testing was carried out at 85 °C and 9 V (1.43VR) for 1000 hours. As a result of these tests (see Fig. V.1) two samples failed in group 1 and 3 samples failed in group 4. Three samples in group 2 had significant current spikes reaching hundreds of microamperes, indicating powerful scintillation events. Group 3 capacitors did not have failures or scintillations, but initially, the currents increased gradually for a few hours reaching hundreds of microamperes, then decreased slowly to the level of a few microampers after 400 hours.

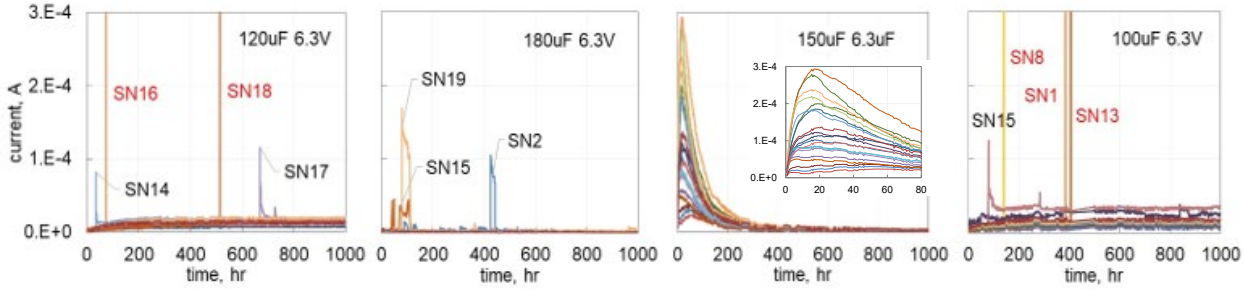

Fig. V.1. Monitored leakage currtents during HALT at 85 °C and 1.43VR for four groups of APCs rated to 6.3 V. Serial numbers in red font indicate failures caused by blown fuses and in black font to scintillation events.

Results of post-HALT measurements of AC characteristics and leakage currents are shown in Fig. V.2. Median values of capacitance decreased by 9% in group 2 and 3 and only by 1 to 2% for capacitors in group 1 and 4. These results are likely due to moisture desorption during HALT. Median values of DF increased more significantly, by 67% and 57% for groups 1 and 4, and approximately two times in groups 2 and 3. Median values of ESR increased substantially, in 10 to 15 times, for all groups. Note, that approximately 20% of the parts had initial ESR values outside the specified limits.

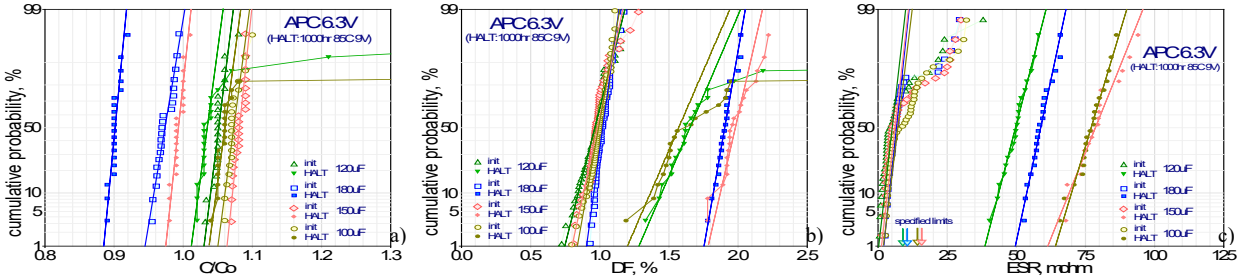

Fig. V.2. Effect of a 1000-hour HALT at 85 °C and 9 V (1.43VR) on capacitance (a), DF (b), and ESR (c) for APCs rated to 6.3 V.

After 1000 hours at 85 °C and 9 V all samples in groups 2 and 3 had acceptable characteristics, and only 10% of samples in group 1 and 15% in group 4 failed. Samples that remained functional after 9 V HALT were used for additional stress testing at 85 °C and 11 V (1.75VR) for 710 hours. At these conditions, all samples in groups 1 and 4 failed within one hour of testing. Variations of leakage currents during 11 V HALT for groups 2 and 3 are shown in Fig. V.3. Leakage currents in group 2 capacitors were unstable, but decreased with time and stabilized after ~200 hours. Six out of 20 samples failed within first 24 hours of testing, but no more failures were detected for the next 690 hours. Two out of six failed samples were the parts that exhibited scintillation events during 9 V HALT, and for this reason powerful scintillations can be considered as failures. Leakage currents in group 3 capacitors increased with time with a hump after a few hours of testing, but no current spiking or failures were observed. The presence of humps in these parts might be associated with additional oxide formation that was observed also in wet aluminum electrolytic capacitors [23].

Distributions of resistances measured after 11 V HALT (Fig.V.3.c) show that all samples in groups 1 and 4 failed short circuit with a median resistance of less than 20 ohms, whereas 40% of group 2 and all parts in group 3 had resistances exceeding 10 Mohm. After HALT, capacitance in group 3 decreased by 17% compared to the initial values, DF increased by 83%, and ESR increased approximately tenfold. Leakage currents post HALT at 9 and 11 V had a tendency of increasing with the higher stress voltage in groups 1 and 4 and decreasing for groups 2 and 3 (see Fig.V.3.d). This is likely due to the differences in manufacturing processes, e.g. oxide formation, or cathode materials used.

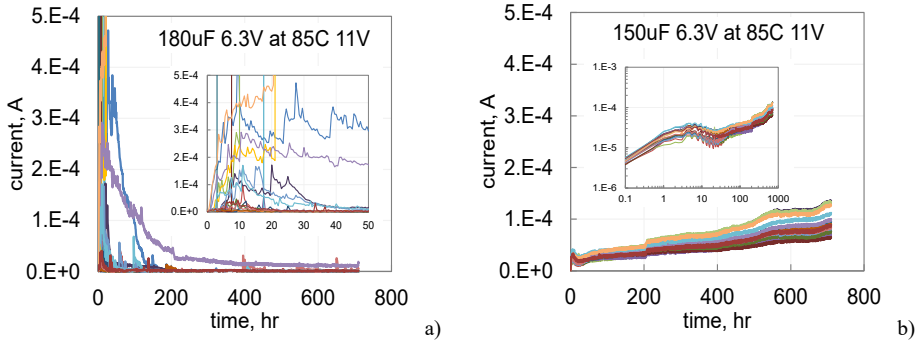

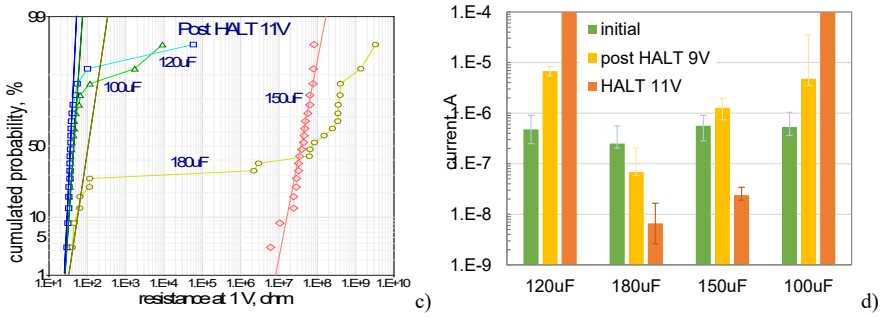

Fig. V.3. Leakage currents during HALT at 85 °C and 1.75VR for gr.2 (a) and gr.3 (b) capacitors. Figure (c) shows distributions of resistances after HALT at 11 V and figure (d) illustrates variations of leakage currents after different HALT conditions. Insets in figures (a) and (b) show the same I-t curves in different scales.

Due to a wide range of TTF for different groups of capacitors, HALT-2 was carried out at 85 °C and 10 V for groups 1 and 4, and at 12 V for groups 2 and 3 capacitors. Results of these tests are shown in Fig. V.4. Most failures (90%) in group 1 (120 µF) occurred by 100 hours and in group 4 (100 µF) by 30 hours of testing. Results for group 2 (180 µF) were similar to HALT at 11 V: majority of the parts (70%) failed by 1 hour, and all capacitors, except for one sample that remained functional through the testing, failed by 7 hours. TTF distributions in Weibull coordinates for groups 1 and 4 capacitors were bymodal indicating the presence of infant mortalty (IM) and WO failures. All groups had samples deviating from WO distributions to longer times forming a group of so-called anti-WO failures. No failures were observed in capacitors from group 3 (150 µF), but leakage currents in these parts had spikes as shown in Fig. V.4.b. Post-HALT-2 measurements of resistances (see Fig. V.4.c) indicate that approximately half of samples from groups 1 and 4 and 90% of samples from group 2 failed hard short circuit with resistances below 100 ohm. The rest of parts had resistances in the kohm range. This indicates that some samples can decrease leakage currents even after powrfull scintillations causing opening of 62 mA fuses. Group 3 capacitors that did not have failures had leakage currents in the microampere range, and respectively, their resistances were in the megaohm range.

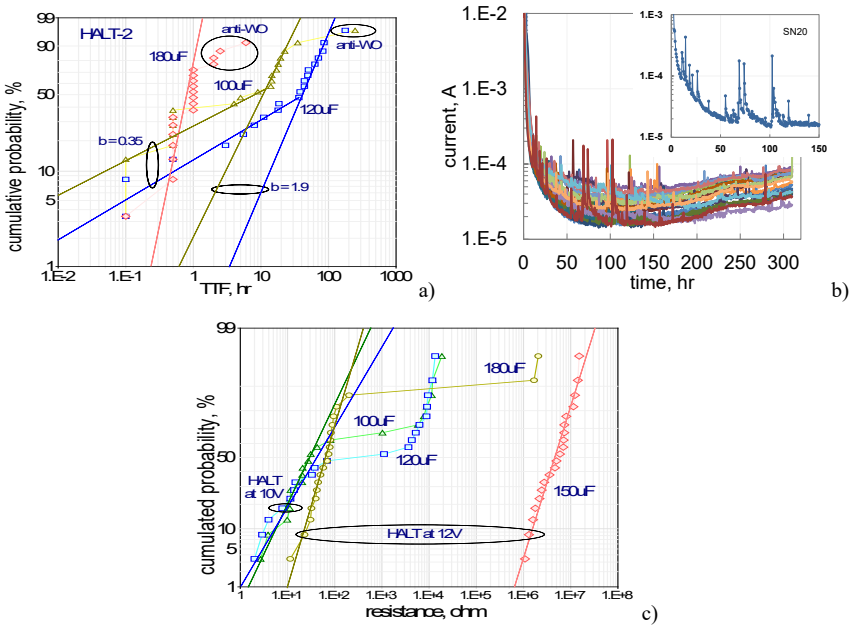

Fig. V.4. Distributions of times to failure during HALT-2 (a), variations of leakage currents for gr.3 (150 µF) capacitors (b), and distribution of resistances measured after HALT-2 (c). Inset in Fig.(b) shows an example of spiking in SN20. Note that actual values of maximum currents during spikes are likely much higher than the ones detected during scanning every 15 min.

Capacitance values after HALT-2 decreased on average by 15% and 25% in groups 2 and 3, whereas capacitance for half of the samples in groups 1 and 4 remained stable, but incresed up to 3.5 times for the rest of the samples. Increased capacitance values were expected for samples with low resistances. Dissipation factor in group 1 and 4 capacitors increased from 10 to 100 times. For half of the group 2 samples, the DF increase was ~20 times, but for group 3

capacitors DF had risen by only 50%. The values of ESR increased in all parts between 10 to 20 times. Results show that the most sensitive to degradation parameters are DF and ESR, and their increase in many cases resulted in parametric failures of the parts.

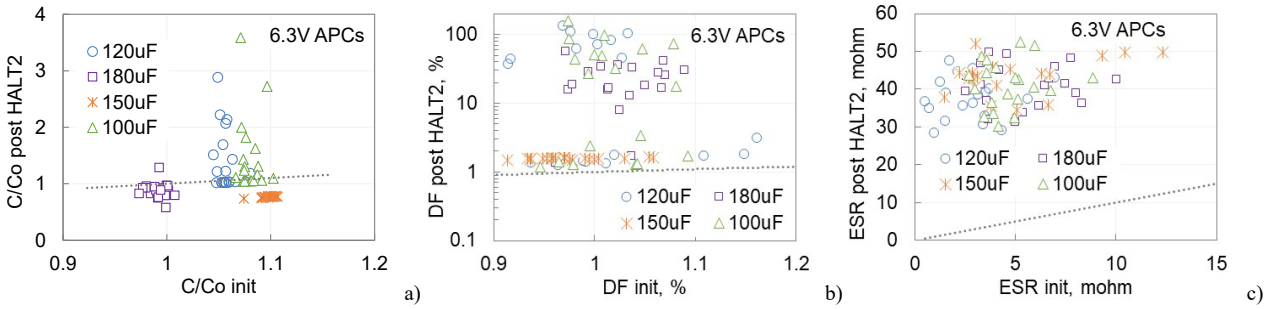

Fig. V.5. Correlation of AC characteristics measured before and after HALT-2. Dotted lines correspond to no change values.

Considering that the level of stress during HALT-2 was excessive for all part types except for gr.3, HALT-3 was carried out at 85 °C and 9.5 V (1.51VR) for 120 µF and 100 µF capacitors and at 11.5 V (1.83VR) for 180 µF and 150 µF capacitors. Similar to the previous HALT conditions, most failures in group 2 parts (~80%) occurred early, by 2 hours of testing, but 4 samples remained operational till the end of test at 1100 hours (Fig. V.6.a). Except for the first two initial failures, majority of the parts follow Weibull distribution with the slope 1.6 indicating WO failures. The 4 samples that did not fail after 1100 hours belong to the anti-WO group. Currents in these samples, although unstable and exhibiting scintillation breakdowns, decreased gradually with time (see Fig.V.6.b).

Group 3 samples (150 µF) as in the previous case, had no failures and the current spikes were much less substantial compared to HALT-2 and to group 2 capacitors during HALT-3 (Fig.V.6.b). This indicates a strong dependence of the probability of scintillations on the voltage stess. Median times to failure during HALT-3 at 9.5 V were 430 and 150 hours respectively for 120 µF and 100 µF capacitors. In some cases, failures occurred after powerfull scintillation events with currents recovering after dozens of hours of testing (see SN20 of 120 µF and SN14 of 100 µF capacitors in Fig. V.6.c). However, similar events might not result in short circuit failures even after several scintillations as shown for SN14 of 120 µF APCs.

After HALT-3, leakage currents were monitored at rated voltage and 20 °C for one hour. The currents increased in different groups from 10 to 30 times compared to the initial values, but no spiking was observed.

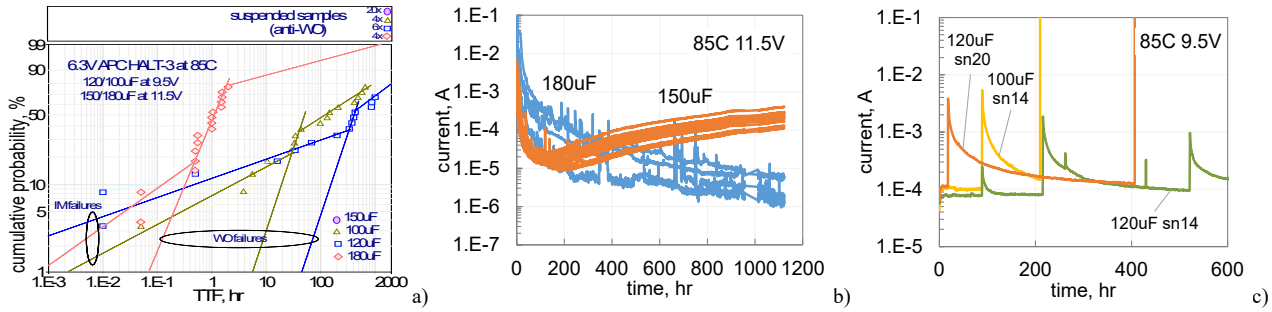

Fig. V.6. Distributions of times-to-failure for three part types (a), leakage currents measured during HALT-3 at 85 °C and 11.5 V for gr.2 and 3 capacitors (b), and examples of scintillation current spikes in gr. 1 and 4 capacitors tested at 9.5 V and 85 °C (c).

To get a better understanding of the behavior of APCs during HALT, currents in all 7 groups of capacitors were monitored for 1000 hours at 125 °C using 10k current sense resistors instead of fuses. Five samples in each group of capacitors rated to 6.3 V and 15 samples for capacitors rated to higher voltages (groups 5, 6, and 7) were used for this study. Capacitors rated to 6.3 V were tested at 9 V (1.43VR), capacitors rated to 10 V were tested at 1.4VR, and capacitors rated to 25 and 35 V were tested at 1.2VR.

Results of 125 °C testing for 6.3 V capacitors are displayed in Fig. V.7. No short circuit failures were detected in any of the groups; however, all parts, except for group 3 (150 µF) exhibited current spikes. During scintillation events, the currents increased sharply typically by 1 to 3 orders of magnitude, and then decreased gradually, for hours, to the

initial level. Considering that the proportion of samples with current spikes during HALT at 85 °C and 9 V was ~15% only (see Fig.V.1), rising HALT temperature increases the probability of scintillations.

Capacitance after HALT at 125 °C decreased by 3 to 7% in all groups except for groups 2 and 3 where the decrease was ~20%; DF increased by 20 to 70% in all groups except for groups 1 and 4, where the rise was 5 and 12 times, and group 5 where DF decreased ~50%. The values of ESR increased on average from 5 to 7 times in all types of capacitors except for group 5 (33 μF 10 V) where the increase was relatively small, ~10%.

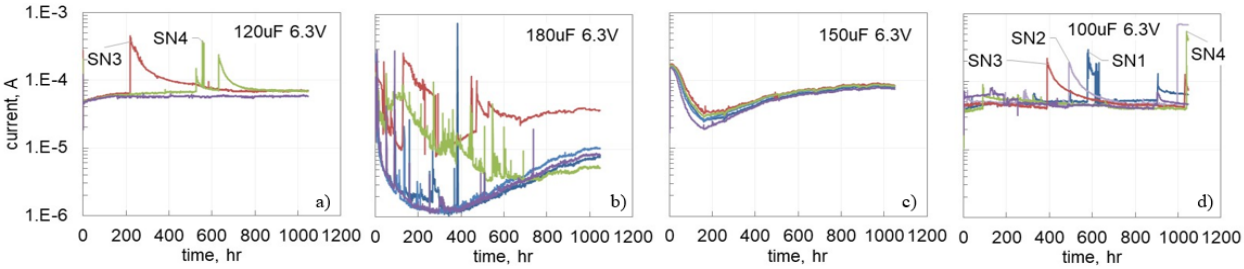

Fig. V.7. Leakage currents in APCs rated to 6.3 V during HALT at 125 °C and 1.43VR.

Spikes of leakage currents during HALT were also observed in capacitors rated to 10 V and above (Fig.V.8). The spiking started after a certain incubation period (typically after more than a dozen of hours) that is required to accumulate defects in the dielectric before scintillation breakdowns occur. In all cases, similar to 6.3 V capacitors, the currents increased sharply by orders of magnitude and then gradually, within hours, relaxed to the initial or some times higher levels. A similar behavior was also observed in PTCs, but in many cases in tantalum capacitors the spiking was due to gradual increasing of currents that followed by a sharp decrease to the initial levels [24]. A fast increase is due to a short duration of the scintillation events that, based on oscilloscopic measurements during CCS testing, occurs within milliseconds. The termination of scintillations is due to self-healing processes that may take hours to complete.

A commonly used self-healing model that assumes a conversion of conductive polymers into high resistive state, caused by local overheating during scintillation to above 300 °C [1, 2, 25], cannot explain this behavior. It is possible that similar to what was suggested for PTCs, local overheating during scintillations changes the distribution of charges trapped in deep states of the dielectric or dielectric/conductive polymer interface, thus subtantially reducing the barrier for the charge flow [15]. Over time, the current refills empty states, increases the barrier, and reduces the leakage.

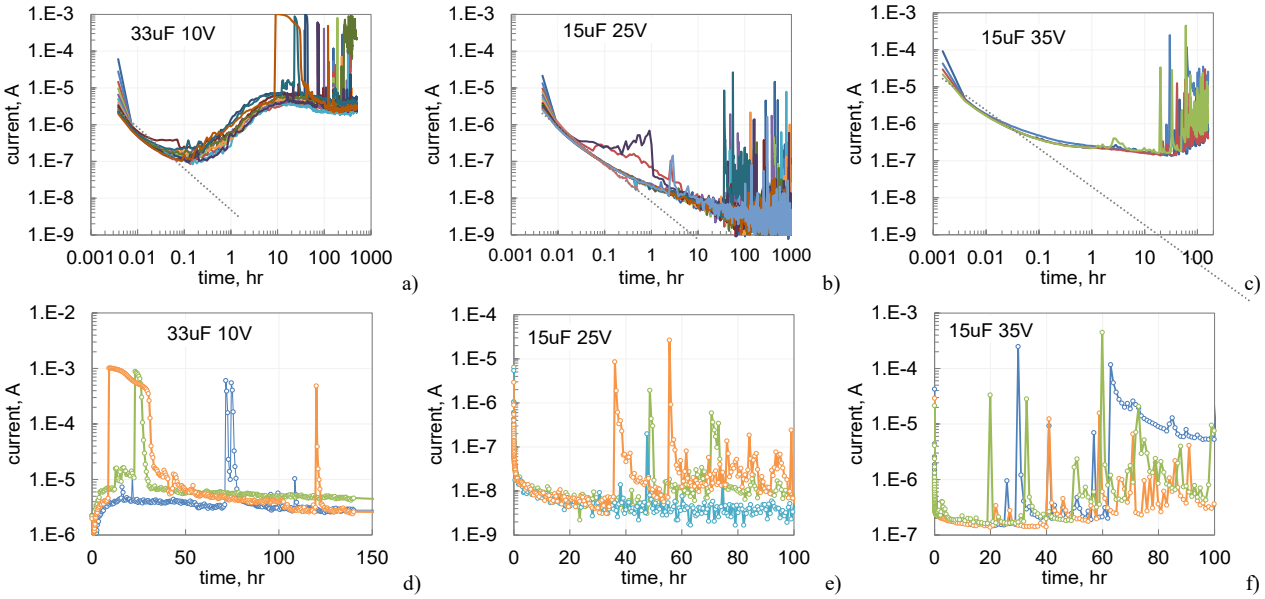

Fig. V.8. Leakage currents in different types of APCs during HALT at 125 °C. Capacitors rated to 10 V (a) were stressed at 1.4VR, and capacitors rated to 25 V (b) and 35 V (c) at 1.2VR. Figures (d – f) show examples of current spikes observed during the testing.

Samples that passed HALT were tested for breakdown voltages using a CCS technique. Average normalized values of VBR are compared with the values for dry, virgin samples (initial) in Fig. V.9 and indicate increasing VBR caused by HALT. Note that the observed rise of VBR (up to 30%) exceeds substantially the coefficient of variations (below 5%) and cannot be explained by survival of parts that had higher levels of VBR initially. This rise is likely due to additional anodic oxidation caused by water molecules remaining in the system even after prolonged operation at 85 °C and may explain the anti-WO phenomena.

The characteristic times to WO failures are plotted against stress voltages during HALT in Fig. V.9.b. The values of normalized breakdown voltages were also used assuming TTF of ~ 10 sec, which is an average duration of CCS testing. In semi-logarithmic coordinates, the data can be linearized indicating an exponential dependence of $TTF_c(V)$ that can be derived from the thermochemical time dependent dielectric breakdown (TDDB) model [26]:

$$TTF_c(V) = t_0 \times \exp\left(-B\frac{V}{VR}\right) \quad ,$$

where t_0 and B are constants.

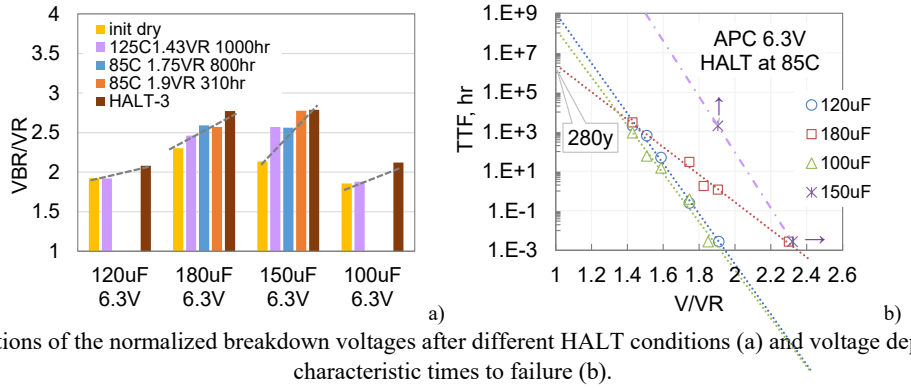

Fig. V.9. Variations of the normalized breakdown voltages after different HALT conditions (a) and voltage dependence of the characteristic times to failure (b).

The values of voltage acceleration constant B for parts shown in Fig. V.9.b vary from 16 for 180 µF to 29 for 120 µF capacitors, which are substantially greater than for PTCs [27]. Extrapolations to the rated voltage indicate that the characteristic times of WO failures at 85 °C exceed 280 years. Assuming that the time to inception of WO failures, (TTF_i) or useful life of the parts, corresponds to the probability of failure of 0.1 %, this time can be calculated based on the characteristic TTF and the slope of Weibull distributions (β):

$$TTF_i(VR) = TTF_c(VR) \times [-\ln(0.999)]^{1/\beta} \quad ,$$

Considering that the slopes are in the range from 1.6 to 2.8, the useful life of the parts exceeds 3 years of operation at 85 °C and at 6.3V. However, voltage derating to 4 V will make this time practically endless, more than 5,000 years.

VI.Summary

Analysis of the performance of 7 types of aluminum polymer capacitors with rated voltages from 6.3 to 35 V, encapsulated in plastic cases with the same footprint, EIA 7343, and manufactured by four different vendors showed that their behavior and reliability differ substantially. Assuring proper storage, handling, screening, lot acceptance testing, and derating, some types of APCs can be used in spaceflight applications.

1) Behavior of the parts during high temperature storage is similar to polymer tantalum capacitors, PTCs, and results in decrease of capacitance and increase of DF and ESR.
   a) All part types failed ESR after a few hundreds of hours at 150 °C, but no parametric failures (increase above 3 times of the specified value) were detected after 1000-hour storage at 125 °C.
   b) Storage at temperatures exceeding 100 °C resulted in increased DCL, approximately an order of magnitude after 3000 hours at 125 °C and up to 3 orders of magnitude after 2000 hours at 150 °C. However, the currents remained within the specified limit after 4000 hours of storage at 100 °C.
   c) Breakdown voltages reduced by 2 to 12% after HTS100 for all part types, and by 3 to 25% after HTS125 for 5 out of 7 types of capacitors.
   d) Three cycles of reflow soldering at T_{max}= 235 °C did not degrade leakage currents but reduced breakdown voltages by ~10% in capacitors rated to 6.3V.

e) Contrary to PTCs, no anomalous charging currents (ACC) were observed in any of the tested APCs initially or after HTS.
f) Activation energy of HTS failures calculated based on capacitance or ESR degradation is 0.73 ±0.16 eV, which is close to the PTC values. Extrapolations of times to failure observed in the range from 100 to 150 °C to operating conditions (65 °C) indicate TTF in the range from 6 to 48 years. Similar to PTCs, successful testing in air at 125 °C for 1000 hours will assure significantly longer (more than 20 years) operational times in vacuum.

2) Storage in humid environments at 85% RH and 85 °C for 850 hours resulted in parametric failures for 2 out of 7 part types, but no significant degradation or failures were detected during storage at 85 °C and 60% RH for 560 hours. The latter condition may be sufficient to assure reliable applications of APCs during terrestrial testing and integration periods.
a) After storage at 85 °C and 85% RH, different types of APCs increased capacitance by 5 to 35%, DF in 2 to 15 times, but there were no significant changes of ESR for all parts except for 150 μF 6.3 V capacitors where ESR increased more than 8 times.
b) Contrary to PTCs, where leakage currents reduce in the presence of moisture due to suppressed anomalous transients, leakage currents in APCs increased up to 100 times after storage at 85 °C and 85% RH for 5 out of 7 part types, but less than 10 times after storage at 85 °C and 60% RH. The excessive leakage currents after storage in humid environments decrease gradually with time under bias to the levels lower than the initial currents.
c) Breakdown voltages increase in the presence of moisture in all tested types of APCs from 8 to 35% after storage at 85% RH and from 3 to 19% after storage at 60% RH. This increase was likely due to additional anodic oxidation in the process of breakdown measurements.

3) Monitored HALT at 85 °C and voltages ranging from 1.4VR to 1.9VR showed that reliability of different types of capacitors rated to 6.3 V varied from 90% of samples failing before 30 hours at 10 V in 100 μF capacitors to no failures after 1100 hours at 11.5 V for 150 μF parts.
a) Similar to tantalum, APCs have infant mortality, wear-out, and anti-WO failures. The latter is due to increasing of breakdown voltages (from 8 to 30% for different part types) during HALT. The presence of IM failures indicates the need for burn-in screening.
b) Dependence of the characteristic times-to-failure on stress voltage can be described using an exponential thermochemical TDDB model with high voltage acceleration constants B (from 16 to 29 for different part types), which is substantially greater than for TPCs.
c) Estimated TTF_c values at 85 °C and VR exceed 280 years and useful life determined at 0.1% of wear-out failures at 85 °C and voltages derated to below 65% VR would exceed thousands of years.
d) The intensity of current spikes during HALT caused by scintillation breakdowns increases with time, temperature, and the level of voltage stress. Group 3 capacitors (150 μF 6.3V) had no failures at all used HALT conditions and contrary to other types, had minimal or no current spiking indicating that APCs can be used reliably in space systems.

VII. Acknowledgment

The author is thankful to Chris Tiu, NASA GSFC Code 562 Associate Branch Head for his review and discussion and to Peter Majewicz, NASA NEPP Program Manager, for his support on this study. This work could not have been done without help of the GSFC Parts Analysis Lab specialists.

VIII. References

[1] J. D. Prymak, "Improvements with polymer cathodes in aluminum and tantalum capacitors," in *APEC 2001. Sixteenth Annual IEEE Applied Power Electronics Conference and Exposition (Cat. No.01CH37181)*, 2001, 4-8 March 2001, pp. 1210-1218 vol.2.
[2] L. L. Macomber, "Solid polymer aluminum capacitor chips in DC-DC converter modules reduce cost and size and improve high-frequency performace," presented at the PCIM Power Electronics 2001, Rosemont, IL, 2001. https://www.cde.com/resources/technical-papers/spa2.pdf
[3] Murata. (2022). *Polymer Aluminum Electrolytic Capacitors*. Available: https://www.murata.com/en-us/products/capacitor/polymer

[4] V. B. Steffen Buhrkal-Donau, Thomas Ebel, "A way to High Voltage Polymer Aluminium Electrolytic Capacitor," presented at the PCNS'21, Milan, It, 2021.
[5] S. Neupane, O. E. Olawale, V. Adashkevich, *et al.*, "Long-term testing results of a high-performance 450 V Polymer Aluminum Electrolytic Capacitor," in *2023 25th European Conference on Power Electronics and Applications (EPE'23 ECCE Europe)*, 2023, 4-8 Sept. 2023, pp. 1-6.
[6] Panasonic. (2022). *SP-CAP™ POLYMER ALUMINUM*. Available: https://na.industrial.panasonic.com/products/capacitors/polymer-capacitors/lineup/sp-cap-polymer-aluminum
[7] KEMET. (2023). *KEMET A798 Plus Performance Aluminum Organic Capacitor AO-CAP®*. Available: https://www.kemet.com/en/us/technical-resources/kemet-a798-plus-performance.html
[8] U. Merker, "Reaching the Next Level of Reliability for Polymer Capacitors," presented at the PCNS'21, Milan, It, 2021.
[9] F. PUHANE. (2020). *ANP071: Aluminum Electrolytic vs. Aluminum Polymer Capacitor*. Available: https://community.element14.com/products/manufacturers/wuerth-elektronik/w/documents/3740/anp071-aluminum-electrolytic-vs-aluminum-polymer-capacitor
[10] Panasonic_Reliability. (2022). *Safety and Legal Matters to Be Observed*. Available: https://api.pim.na.industrial.panasonic.com/file_stream/main/fileversion/2464
[11] A. Shrivastava, M. H. Azarian and M. Pecht, "Rapid Assessment Testing of Polymer Aluminum Electrolytic Capacitors in Elevated Temperature–Humidity Environments," *Journal of Failure Analysis and Prevention,* vol. 16, pp. 1059-1066, 2016/12/01 2016 https://doi.org/10.1007/s11668-016-0184-0
[12] J. Romero, M. H. Azarian and M. Pecht, "Reliability analysis of multilayer polymer aluminum electrolytic capacitors," *Microelectronics Reliability,* vol. 112, p. 113725, 2020/09/01/ 2020 https://www.sciencedirect.com/science/article/pii/S0026271419311266
[13] D. Liu, "NEPP report: Physical and Electrical Characterization of Aluminum Polymer Capacitors," 2009, https://nepp.nasa.gov/files/20389/09_005_GSFC_Williams_Liu%20APC%20Final%20Report.pdf
[14] A. Teverovsky, "Guidelines for Screening, Lot Acceptance, and Derating for Polymer Tantalum Capacitors," NASA STI Program, Greenbelt, MD, NEPP report 2023, https://ntrs.nasa.gov/api/citations/20220019033/downloads/20220019033-Teverovsky-2023-NASA-TP-Guidelines-Screening-PTC_v3.pdf
[15] A. Teverovsky, "Breakdown and Self-healing in Tantalum Capacitors," *IEEE Transactions on Dielectrics and Electrical Insulation,* vol. 28, pp. 663-671, 2021
[16] A.Teverovsky, "Metrics for Anomalous Charging currents in Polymer Tantalum Capacitors," in *2023 IEEE Electrical Insulation Conference (IEC)* Quebec City, Quebec, Canada, 2023, 18 June - 21 June 2023, pp. 169-173.
[17] A. Teverovsky, "Effect of High Temperature Storage on AC Characteristics of Polymer Tantalum Capacitors," in *International Conference on High Temperature Electronics (HiTec - iMAPS)*, virtual, 2021, April 26-29.
[18] A. Teverovsky, "Degradation of Aluminum and Tantalum Wet Electrolytic Capacitors during High Temperature Storage," in *4th PCNS Passive Components Networking Symposium*, Sønderborg, Denmark, 2023, September 11-13, pp. 129-140.
[19] K. Iida. (2023). *Essential Characteristics of Capacitors. DC leakage current.* Available: https://www.aictech-inc.com/en/valuable-articles/capacitor_foundation05.html
[20] A. Teverovsky, "Effect of Moisture on AC Characteristics of Chip Polymer Tantalum Capacitors," *IEEE Transactions on Components, Packaging and Manufacturing Technology,* vol. 9, pp. 2282-2289, 2019
[21] A. Teverovsky, "Breakdown and Self-healing in MnO2 and Polymer TantalumCapacitors," NASA STI Program, Greenbelt, MD, NEPP report 2021, https://nepp.nasa.gov/docs/tasks/003-Evaluation-Polymer-Tantalum-Capacitors-for-Space-Applications/2020-NASA-TM-Teverovsky-MnO2-Polymer-Tantalum-Capacitors-20205011704.pdf
[22] E. P. W. Jenkins, S. T. Keene, I. B. Dimov, *et al.*, "High capacitance freestanding PEDOT:PSS electrodes for low-frequency electric field delivery," *AIP Advances,* vol. 14, 2024 https://doi.org/10.1063/5.0180487
[23] A. Teverovsky, "Updates on Capacitors' Tasks," in *2023 Annual Electronic Technology Workshop, NEPP ETW*, Greenbelt, MD, 2023, June 12-15. https://nepp.nasa.gov/docs/etw/2023/14-JUN-WED/1610_Teverovsky_20230008485.pdf
[24] A. Teverovsky, "Evaluation of 10V chip polymer tantalum capacitors for space applications," presented at the ESA 2nd International Symposium - Space Passive Component Days, Noordwijk, The Netherlands, 2016.
[25] Panasonic, "Understanding polymer and hybrid capacitors," *White paper,* 2015 https://www.ttieurope.com/content/dam/tti-europe/manufacturers/panasonic/resources/Whitepaper_PolymerCapacitor.pdf
[26] A. Teverovsky, "Infant Mortality and Wear-Out Failures in Polymer and MnO2 Tantalum Capacitors," in *2022 IEEE International Reliability Physics Symposium (IRPS)*, 2022, 27-31 March 2022, pp. P46-1-P46-9.
[27] A. Eidelman, S. Zlatopolsky and A. Teverovsky, "Acceleration Factors for Reliability Assessment of Polymer Tantalum Capacitors," in *3rd PCNS Passive Components Networking Symposium*, Milan, Italy, 2021, September 7-10, pp. 119-129.

Appendix A. Characteristics of Aluminum Polymer Capacitors

This appendix contains a brief description of information obtained from specifications for aluminum polymer capacitors and experimental data that characterize behavior of APCs.

Analysis of data sheets

Data sheets were analyzed for Murata ECAS series, Panasonic SP series, KEMET AO-CAP series, Wurth Elektronik WCAP series, and CDE XMPL series capacitors. Most chip APCs are rated to voltages below 35 V, have capacitance tolerance of 20%, maximum dissipation factors from 6 to 10%, minimal operating temperature of -55 °C, maximum temperature from 85 °C to 135 °C, and cases size 7343.

Leakage currents are rated based on CV values with the limits that are typically 3 times lower for low voltage (< 10 V) compares to high voltage (≥ 10 V) parts (see Table 2 and Fig.A.1.a). Most manufacturers require 2 minutes electrification, but KEMET required 5 minutes. This allowed KEMET for a reduction of the maximum leakage currents almost two times. Murata and KEMET suggest preconditioning to reduce leakage currents that might rise after a long-term storage.

Table 2. Conditions for DCL measurements

Mfr	Part type	test cond	Rating <10V	Rating >=10V	Comments
Panasonic	SP	2 min	0.1CV	0.3CV	
Murata	ECAS	2 min	0.1CV	0.3CV	Preconditioning: VR through 1k for 1 hr at 105C. Discharge and keep at RT for 4-24hr
Kemet	A700	5 min	(0.04 or 0.06)CV		Preconditioning: VR through 1k for 1 hr at 105C. Discharge and keep at RT for 4-24hr
WE	WCAP	2 min	0.1CV		
CDE	XMPL	2 min	0.1CV	0.3CV	

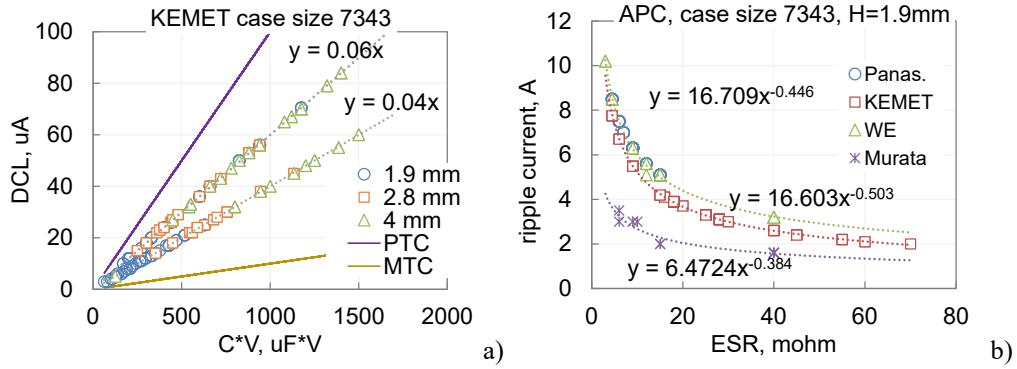

Fig. A.1. Variations of maximum leakage currents vs. CV values for KEMET APCs (marks), MnO2 tantalum capacitors, MTC, and polymer tantalum capacitors, PTC (a) and variations of the maximum ripple currents with ESR for capacitors from different vendors (b).

Apparently, the maximum ripple current values that are shown in Fig.A.1.b are calculated based on maximum ESR, rather than determined experimentally. The difference in ripple current - ESR variations for different manufacturers is likely due to different requirements for possible overheating associated with ripple currents. For example, Panasonic and WE allow temperature rise of 45 °C at 100 kHz, whereas maximum temperature rise for KEMET is 20 °C. Murata does not specify the possible temperature rise.

Storage conditions

All manufacturers are warning about possible degradation caused by a long-term storage in humid conditions that might degrade leakage currents. For some reasons, Panasonic warns also against using APCs under a low atmospheric pressure or depressurized condition. Manufacturers also do not guarantee specified characteristics of the part after from one to 3.5 years of the shelf life.

Panasonic: The storage period before opening the moisture-proof bag is two years after manufacture, and after opening the bag is seven days.

Würth Elektronik: A storage of products for longer than 12 months is not recommended. The maximum storage time after opening the package are 7 days. Baking is not recommended. If the capacitor was stored for a long period of time, it is recommended to apply DC working voltage for 30 minutes through a 1 kΩ protective series resistor.

CDE: When stored at room temperature, in low humidity, and out of direct sunlight, SPA capacitors have a storage life of 42 months. Storage at high humidity over long periods of time can cause the DC leakage current to increase. However, the application of rated voltage will reduce the DC leakage current to normal limits.

MURATA: Term of warranty for this product is two years after packaging in a moisture-proof bag. The capacitors should be kept dry using desiccators or any other methods after unsealing the moisture-proof packaging. If more than one week has passed under the recommended storage environment specified above after unsealing the packaging, it is recommended to bake. Recommended baking is one week at 60 °C.

KEMET: the shelf life for solderability is 12 months after the manufacturing date. While the capacitance, ESR, and impedance remain stable during extended storage, the leakage current may gradually increase over time.

Qualification testing

Different manufacturers have somewhat different stress test conditions and requirements for the post-stress characteristics (see Table 3). These tests include moisture resistance, life test, and shelf-life test. Humidity testing appears to be the most stressful for the parts and requires a substantial relaxing of the requirements. In particular, CDE warns that life expectancy decreases exponentially as RH increases from 35 to 85%.

Table 3. Stress test requirements

Mfr	TEST	Test Conditions	Requirements
Panasonic SX	Damp heat	60C, 90%RH, 500hr	DCL< IL, |ΔC|<(0.5-0.7) x init, DF< 2x init
	Endurance	105C, 2000hr, VR	DCL<3x init, |ΔC|<0.2x init, DF< 2x init
Murata ECSAS	HUM storage	60C, 90-95%RH, 500hr	DCL<3x IL, ΔC<(-0.2 +0.5)x init, DF<2X IL
	HUM bias	60C, 90-95%RH, 500hr, VR	DCL< IL, ΔC< (-0.2 +0.5)x init, DF<2x IL
	Shelf life	105C, 1000hr	DCL< IL, |ΔC|<0.1x init, DF< IL
	Endurance	105C, 2000hr, VR	DCL< IL, |ΔC|<0.2x init, DF< IL
Kemet	HUM storage	60C, 90%RH, 500hr	DCL< 5x init, ΔC<1.3x init, DF< IL
	HUM bias	60C, 90%RH, 1000hr, VR	DCL< 5x IL, ΔC<-0.05/+0.3 x init, DF< IL
	Storage life	105C/125C, 2000hr-3000hr	DCL< 1.25x init, ΔC< 0.1xIL, DF< IL, ESR<2xIL
	Endurance	105C/125C, 2000hr-3000hr, VR	DCL< 1.25X init, ΔC< 0.1xIL, DF< IL, ESR<2xIL
CDE SPA	HUM storage	60C, 90%RH, 500hr	DCL < (1-2)xIL, ΔC < +(0.4-0.7) -0.2xIL, DF < 2xIL
	Loaded life	105C, 2000hr, VR	DCL < (1-3)xIL, ΔC < ±0.2xIL, DF < 2xIL
	Shelf life	105C, 500hr	DCL < IL, ΔC < ±0.1xIL, DF < 2xIL

Note. IL= initial limit; init.= initial value

Note, that most companies do not specify ESR values after stress testing. In KEMET specifications, ESR measurements are not required after humidity testing. Also, for some part series, the duration of storage in humid environments are at least two times less than the duration in similar conditions under bias. This might indicate a

substantial degradation of ESR after stress testing that negates the benefit of using APCs (low ESR). Although the specifications indicate a substantial degradation after exposure to humid environments, our data showed that six out of seven lots had stable ESR values after 850 hours in humidity chamber at 85V 85% RH. Results of this report confirm that in the presence of moisture leakage currents continue decreasing with time under bias. This is most likely due to the anodic oxide growth and continuation of self-healing in the dielectric.

The level of DCL increase after stress testing varies from no change of the limit for Murata ECSAS series to up to 5 times for the capacitors from KEMET. This might be due to the initially higher acceptable level of DCL for Murata capacitors or to increased duration of humidity testing from 500 to 1000 hours for KEMET capacitors.

Experimental data

AC characteristics

Typical frequency dependencies of AC characteristics are shown in Fig.A.1 and distributions of C and DF measured at 120 Hz and ESR measured at 100 kHz are presented in Fig.A.2.

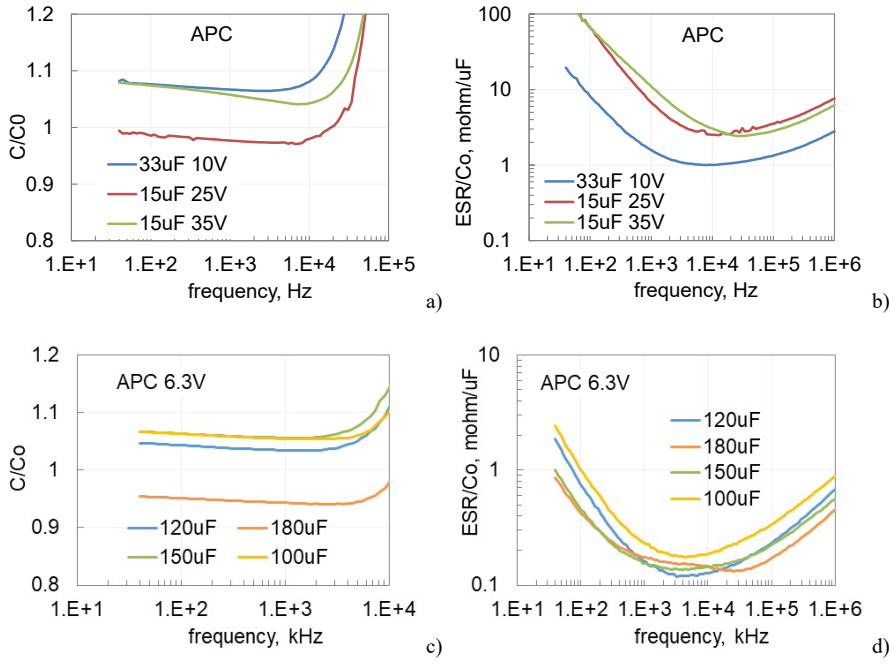

Fig.A.1. Frequency dependencies of normalized capacitance (a, c) and ESR (b, d) for capacitors used in this study.

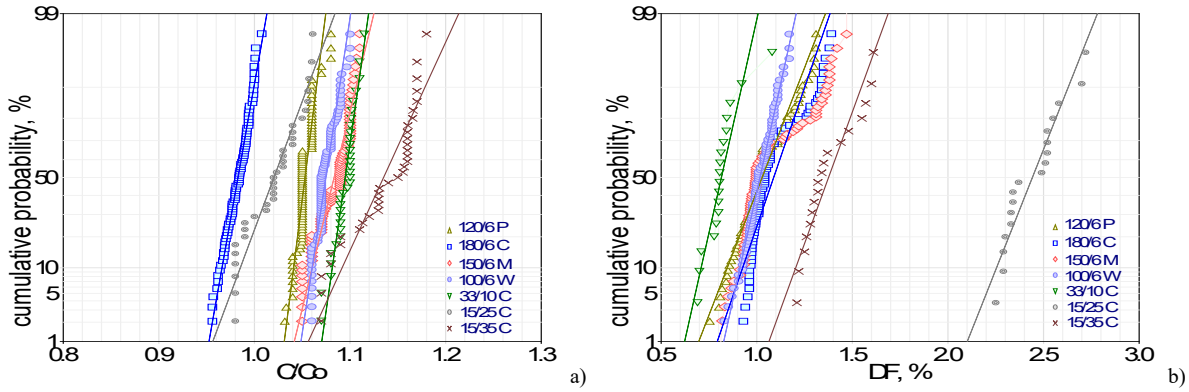

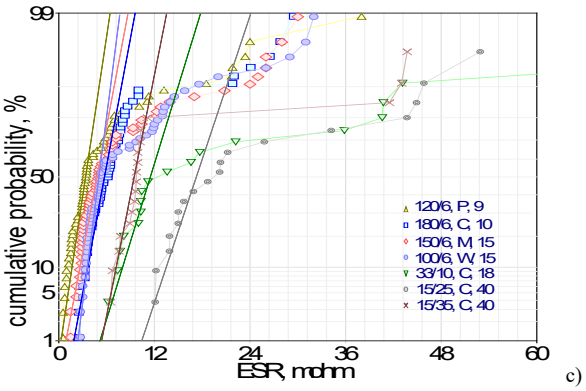

Fig.2. Distributions of normalized capacitances (a), DF (b) and ESR (c) values. Digits in the legend correspond to the specified ESR values in mohm.

For all tested parts, C and DF values were within the specified limits. However, up to 60% of the parts had out-of-family ESR values and up to 10% exceeded the specified limits.

Leakage currents

Variations of polarization (under applied rated voltage) and depolarization (at zero volt followed polarization) with time after voltage application are shown in Fig.A.3. Relaxation of leakage currents followed power function with the exponent *m* close to -1. This behavior, so called Curie – von Schweidler law, is typical for most types of dielectrics and capacitors. Similar absolute values of currents measured during polarization and depolarization for more than 1000 sec indicate a low level of the intrinsic leakage currents that are likely in the nanoampere range and orders of magnitude below the specified limits.

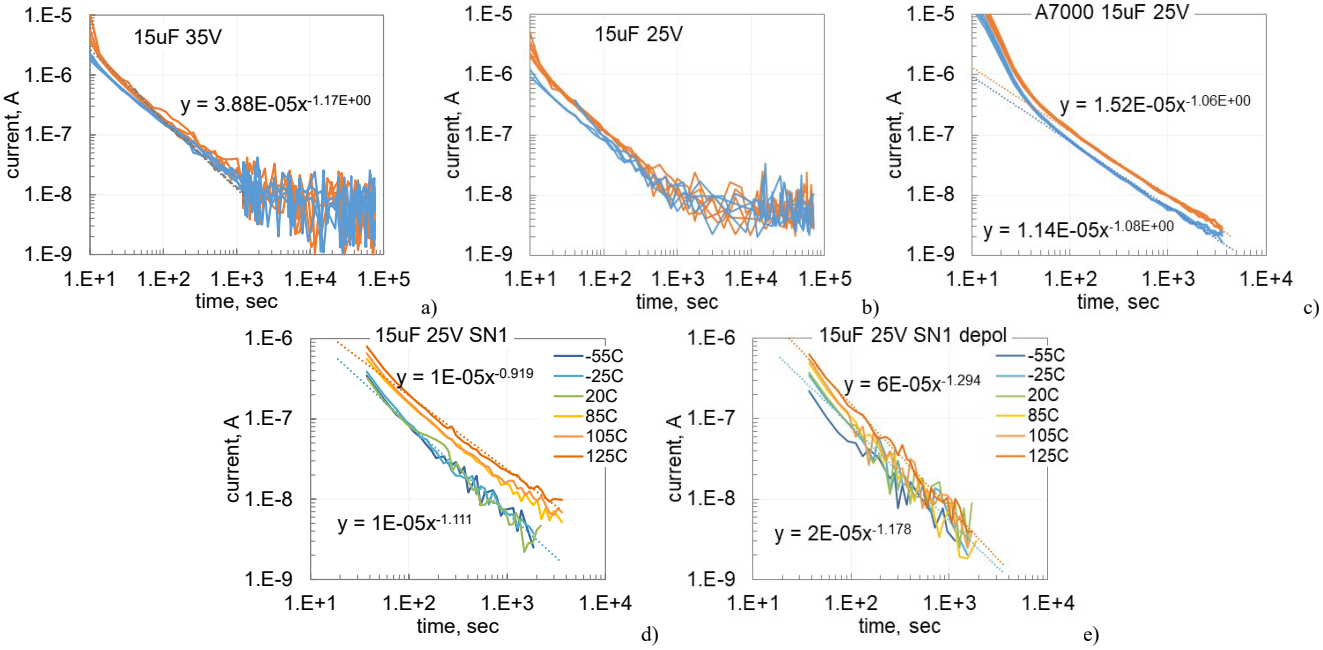

Fig.3. Relaxation of polarization (a, b, d) and depolarization (c, e) leakage currents in capacitors rated to 35 V and 25 V at 20 °C (a-c) and in the range of temperatures from -55 °C to +125 °C. Note that dashed lines in (a, d, and e) correspond to depolarization currents and indicate that the currents measured before 1000 sec are mostly due to absorption processes in the dielectric.

Blue and red curves in Fig.A.3(a-c) correspond to the parts preconditioned in humid (450 hour at 85 °C and 60% RH) and dry (150 hour bake at 100 °C) environments and indicate a small decrease of the transient currents in humid conditions, likely due to anomalous transients. Note that this effect is much more pronounced in PTCs that have variations of leakage currents by orders of magnitude. Also, contrary to PTCs, temperature has a relatively small effect on leakage currents in APCs (see Fig.A.4).

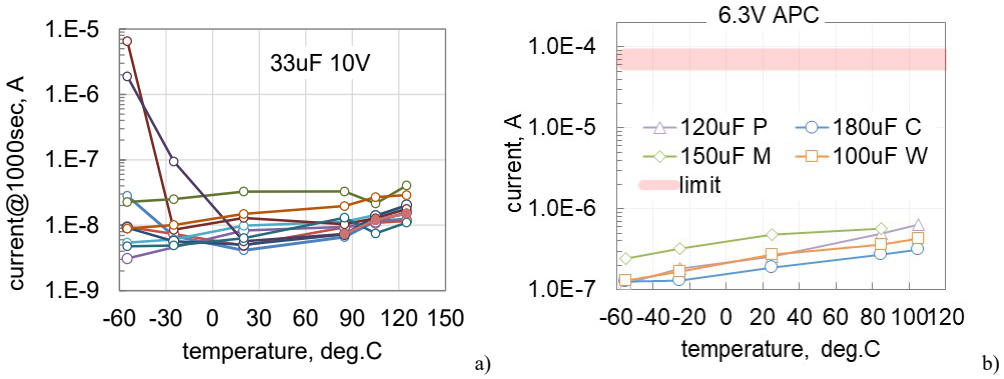

Fig.A.4. Temperature variations of leakage currents measured at 1000 sec of polarization for 33 µF 10 V (a) and capacitors rated to 6.3 V (b).

Two samples of 33 µF 10 V capacitors had anomalously large currents at -55 °C that reduced more than 3 orders of magnitude at higher temperatures (Fig.A.4.a). This behavior indicates the presence of defects that apparently are self-healing with time under bias. Note, that for majority of the parts the currents increased less than an order of magnitude when temperature raised from -55 °C to +125 °C. The latter corresponds to a relatively small activation energy of E_a ~ 0.22 eV for 33 µF 10 V and even lower E_a < 0.1 eV for 6.3 V capacitors.

Variations of polarization and depolarization currents with time for capacitors rated to 6.3 V are shown in Fig.A.5. This figure also shows variations of the absorption charge, Q_t, with voltage, that was calculated as an integral of depolarization currents with time. Variations Q_t with voltage can be approximated with linear functions that allow for calculation of the absorption capacitance, C_t. The results show that C_t values are from 34% to 44% of the nominal capacitance of the part that is more than 50% larger than the absorption capacitance in polymer tantalum capacitors.

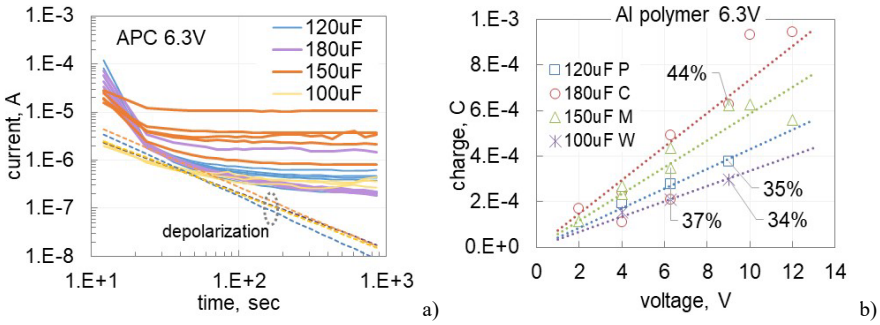

Fig.A.5. Relaxation of polarization and depolarization currents (a) and variation of the accumulated charge with voltage (b). Note, that for 6.3 V capacitors polarization currents were much larger than depolarization currents indicating that the leakage is mostly due to the presence of defects in the dielectric.

Voltage dependencies and distributions of leakage current for different part types are shown in Fig.A.6. I-V characteristics in semilogarithmic coordinates can be approximated with straight lines indicating an exponential dependence of currents on the square root of voltage. This behavior can be explained by the Schottky barrier limited conduction process. Note, that although distributions of leakage currents indicate the presence of the out-of-family samples, they remain within the specified limit (last digits in the legend indicate DCL in µA). This is mostly because the limits are more than 2 orders of magnitude larger than the operational leakage currents. Also, according to specifications, leakage currents in capacitors rated to 10V or more are expected to be at least three times greater than

for low-voltage capacitors. However, according to our data, currents in the low-voltage group are almost an order of magnitude greater than in the high-voltage group.

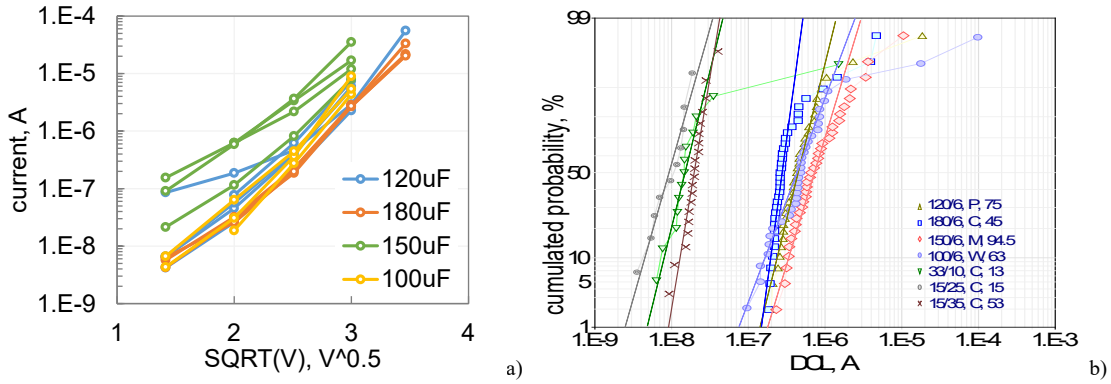

Fig.A.6. Voltage dependence of leakage currents (a) and distributions of leakage currents measured at 20 °C after 1000 sec electrification in APCs rated to 6.3 V (b).

Breakdown voltages

Considering the effect of moisture on breakdown voltages in PTCs, the constant current stress, CCS, testing was carried out using APCs after 1500 hr of storage either at 100 °C (dry samples) or after same time storage at 20 °C and 95% RH (wet samples). Results of these tests for capacitors rated to 10, 25, and 35 V are shown in Fig.A.7 and indicate that the presence of moisture increases VBR. In most cases, except for wet 10 V capacitors, scintillation breakdowns resulted in reduction of resistances to the kiloohms range rather than in short circuits of the parts. The wet 10 V capacitors failed mostly short circuit apparently due to a substantially increased breakdown voltage. Repeat testing confirmed the "leaky conditions" with resistances in kiloohms range at voltages that are below VBR. Wet 25 and 35 V capacitors can sustain multiple scintillation events before failures.

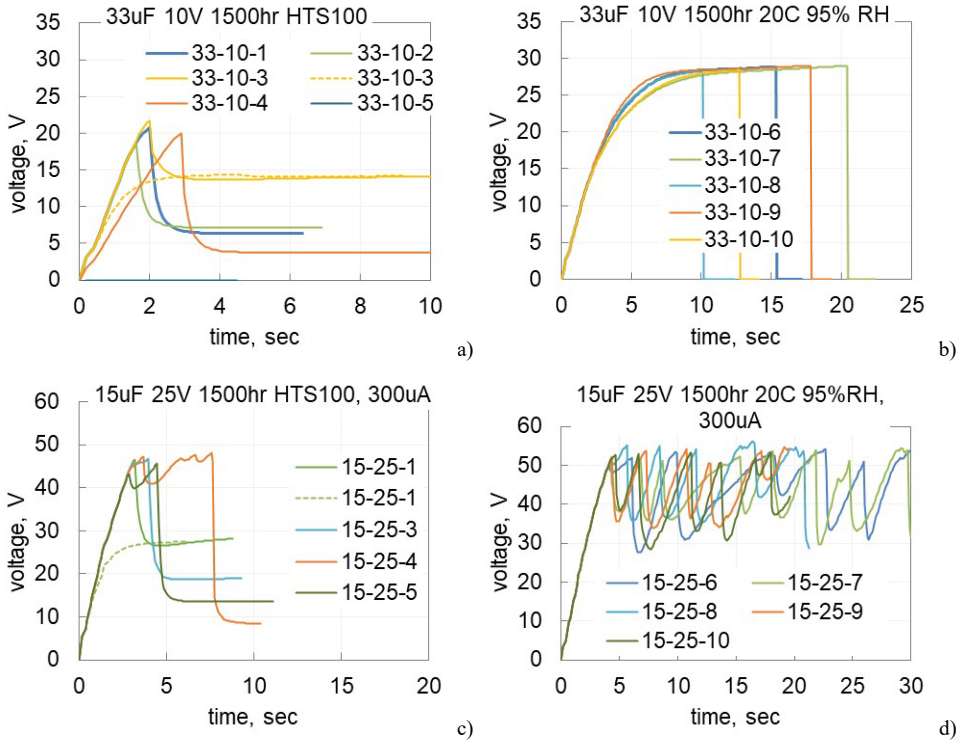

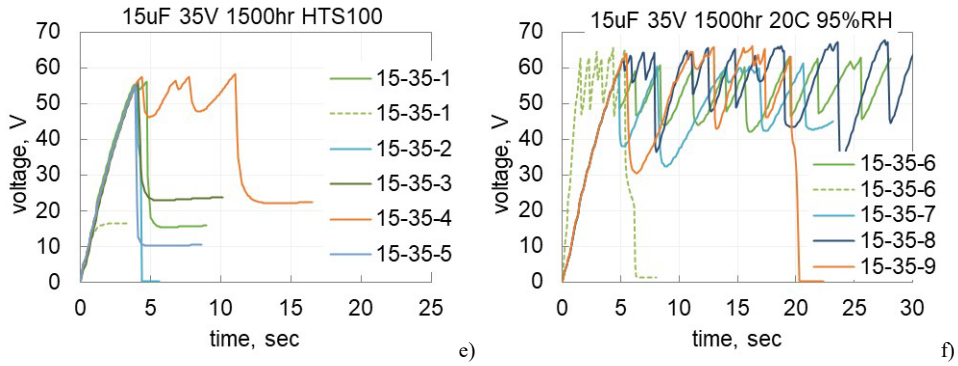

Fig.A.7. Results of CCS testing at currents 0.3 to 1 mA for dry (a, c, e) and wet (b, d, f) capacitors rated to 10 V (a, b), 25 V (c, d), and 35 V (e, f). Dashed curves indicate repeat testing of the sample at the same or increased stress currents.

Results of CCS testing for dry capacitors rated to 6.3 V are shown in Fig.A.8. Similar to the higher voltage ratings, scintillation breakdowns resulted mostly in "leaky" 120 µF and 100 µF capacitors with kiloohms range resistances. Behavior of 180 µF and 150 µF capacitors was different. Variations of voltage across the part stabilized with time of charging at a level $V_{stab}(I_{stress})$ indicating conditions when the stress current, I_{stress}, is equal to the leakage current of the capacitor. Increasing I_{stress} accelerates the charging process, but only slightly increases V_{stab}. A further increase of the stress current results in extremal dependence of V-t variations when voltages are decreasing after reaching maximum that can be defined as a non-destructive breakdown voltage. This decrease is associated with overheating of the parts that increases leakage current and thus decreases V_{stab}. In some cases, at high stress currents the voltage across the part might increase with time again, as shown in Fig. 8c. This behavior indicates a process that causes reduction of leakage current with time at a relatively high temperature and requires additional analysis.

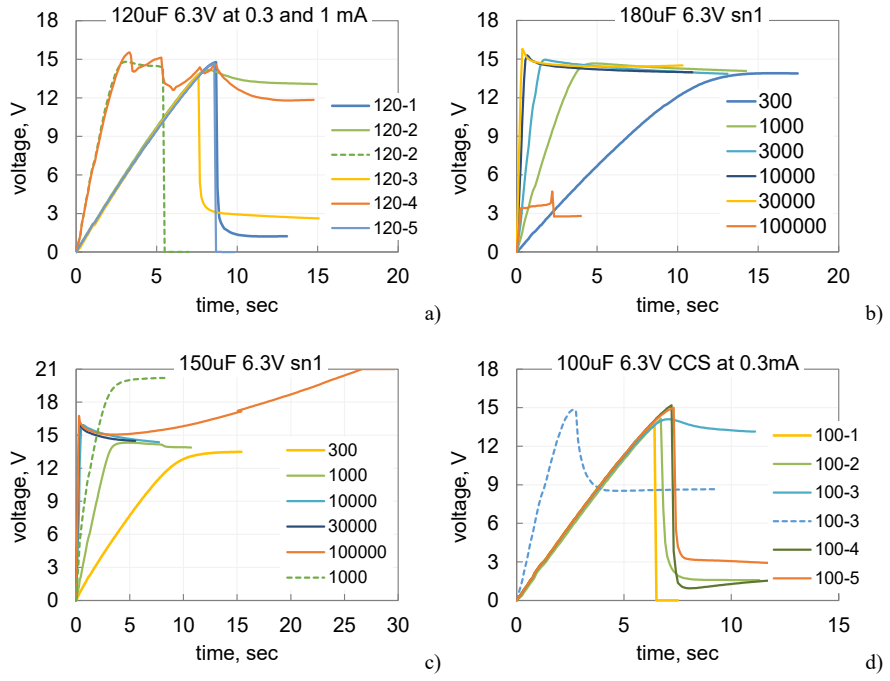

Fig.A.8. Voltage charging processes during CCS testing for different types of capacitors rated to 6.3V. Legends in figures (a) and (d) indicate different samples, and in figures (b) and (c) stress currents in µA. Dashed lines indicate repeat CCS testing.

Distributions of breakdown voltages normalized to the rated voltages for seven types of capacitors used in this study are shown in Fig.A.9.a. Apparently due to a relatively small sample size (20 samples), we do not see low-voltage tails of the distributions that are typically observed in tantalum electrolytic capacitors. Four out of 7 types of capacitors had median breakdown voltages twice higher than the rated voltages. As was expected based on results with PTCs, higher voltage ratings have lower normalized breakdown voltages (Fig.A.9.b.) Capacitors rated to 6.3 V and 180 µF and 150 µF had noticeably larger breakdown voltages compared to 120 µF and 100 µF parts.

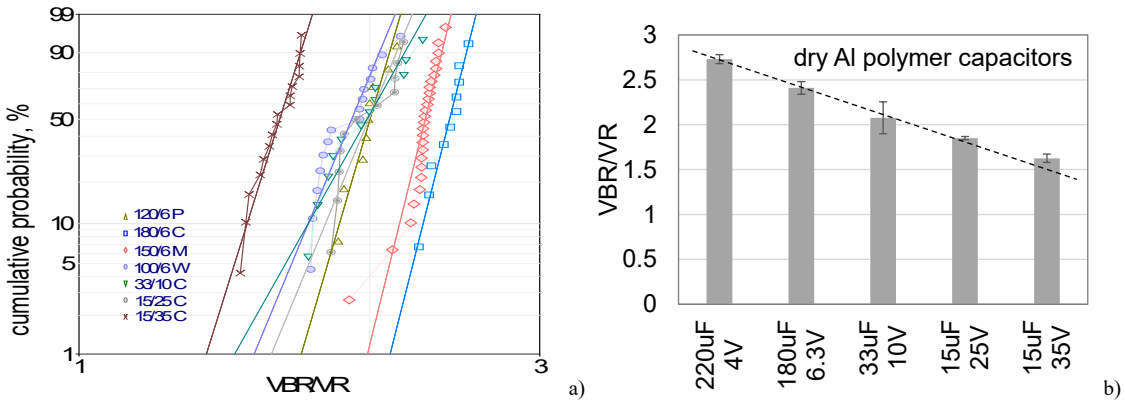

Fig.A.9. Distributions of breakdown voltages in Weibull coordinates (a) and variations of normalized breakdown voltages with the rated voltage (b).

Leakage currents in the "leaky" after CCS testing capacitors were monitored with time at room conditions and rated voltages for 6.3 V and 10 V capacitors and at 10 V for 25 V capacitors. Results of these measurements are shown in Fig.A.10. Leakage currents decreased up to 3 orders of magnitude from dozens and hundreds of microamperes initially to dozens and hundreds of nanometers after hours to hundreds of hours of testing. The currents were not stable, had spikes, and in some cases, the decrease happened by stages when currents reduced repetitively by stages with a relatively short period of time between the stages. A similar behavior was also observed in polymer tantalum capacitors and is likely associated with anomalous transients in polymer cathode capacitors.

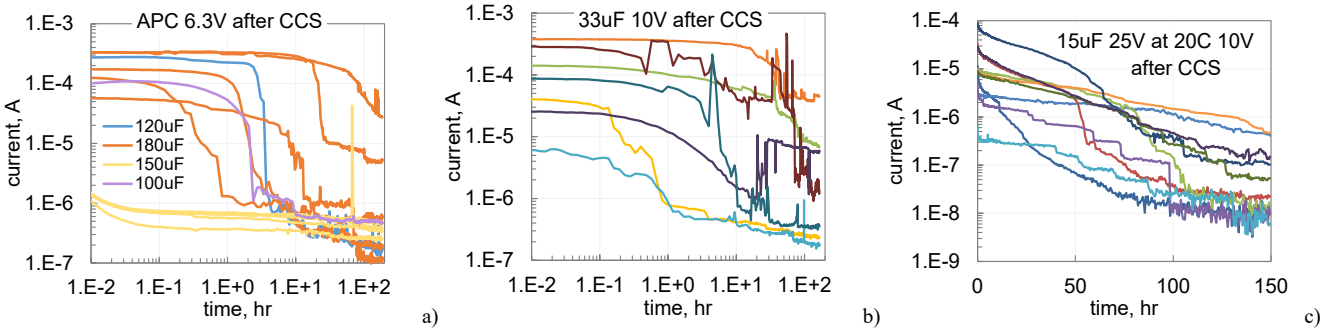

Fig.A.10. Leakage currents in 6.3 V (a), 10 V (b) and 25 V (c) capacitors after CCS testing.

To assess the effect of temperature on breakdown voltages, CCS testing was carried out at 20 °C, 85 °C, and 125 °C for 120 µF and 100 µF capacitors rated to 6.3 V. As evident from Fig.A.11.a, breakdown voltages are decreasing with temperature approximately by 7.5% at 125 °C. Similar to testing at room conditions, the duration of the scintillation events is typically ~ 0.1 msec, but occasionally might last for a few milliseconds (Fig.A.11.b, c). The latter is more likely to result in the "leaky" capacitors.

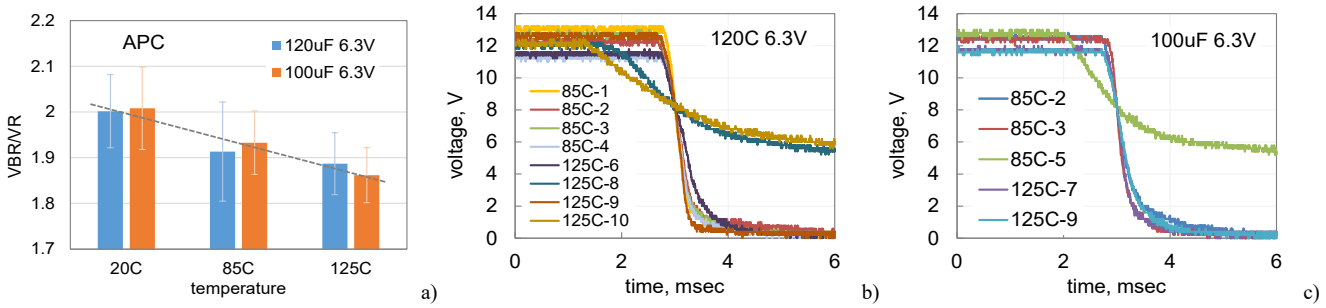

Fig.A.11. Variations of breakdown voltages with temperature (a) and oscillograms of the scintillation events for 120 μF and 100 μF capacitors (b, c).

Effect of reverse bias

For comparative evaluation of behavior of APCs and TPCs under reverse bias, voltages across the capacitors were measured during CCS testing at different stress currents. An examples of CCS testing in the reversed direction is shown in Fig. A.12.a. I-V characteristics for different types of capacitors based on results of these measurements are shown in Fig.A.12.b and c. After a certain threshold voltage that corresponds to conditions when reverse current reaches 0.1 mA, $V_{0.1\,mA}$, the currents increased with voltage exponentially, $I_{RB} \sim \exp(\alpha V)$. This allows to characterize reverse bias behavior using two constants, α and $V_{0.1\,mA}$.

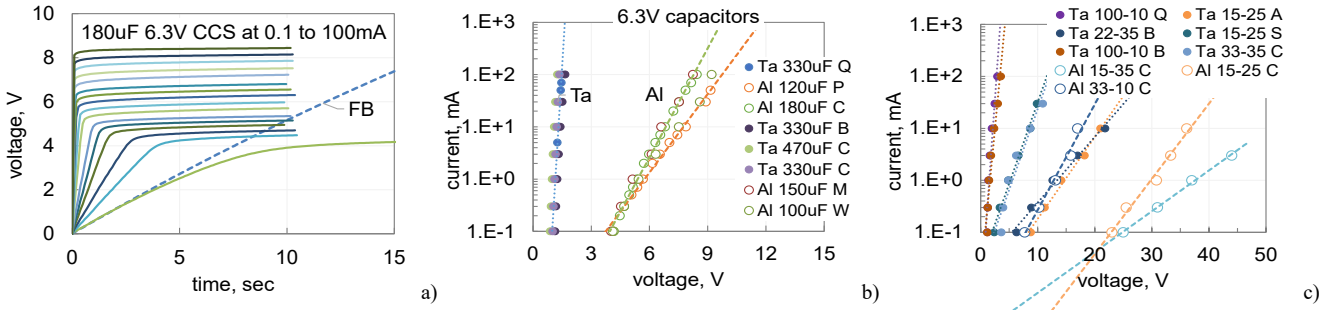

Fig.A.12. Results of reverse bias CCS testing at currents varying from 0.1 mA to 100 mA for 180 μF 6.3 V capacitor (a) and reverse bias I-V characteristics for different aluminum and tantalum polymer capacitors (b, c). For comparison purposes, a dashed line in (a) shows a forward direction charging curve at 0.1 mA.

Results of calculations of α and $V_{0.1\,mA}$ for different types of APCs and PTCs are shown in Fig.A.13. On average, the threshold voltages are greater for aluminum capacitors and the difference increases with voltage rating. The slope α is up to an order of magnitude smaller for low-voltage APCs compared to TPCs. At voltage ratings above 10 V, the difference is slightly reduced, but $V_{0.1\,mA}$ values remain greater for tantalum capacitors. Overall, results indicate that aluminum capacitors can withstand larger reverse voltages compared to tantalum capacitors.

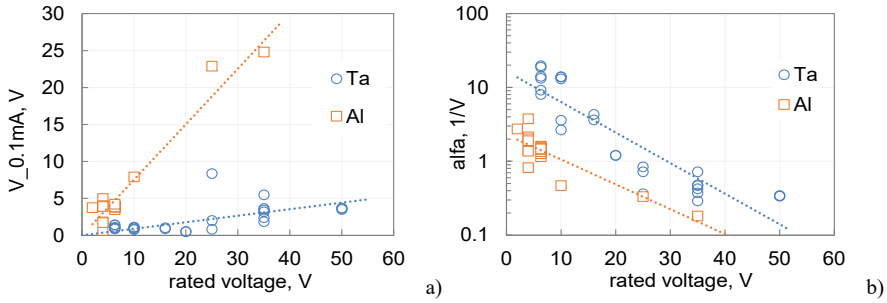

Fig. A.13. Variations of the threshold voltages (a) and slopes of I-V curves (b) for aluminum and tantalum polymer capacitors biased in reverse direction.

Appendix B. Construction Analysis of Aluminum Polymer Capacitors

The parts were manufactured by four vendors with the same footprint, 7.3x4.3 mm, and thickness of the case that varied from 1.9 to 2.8 mm (H) as shown in Table 1.

Table 1. Characteristics of the parts used in this study.

Group	Mfr	C, uF	VR, V	ESR, mohm	DF, %	DCL, uA	T_max	H, mm
1	A	120	6.3	9	6	75	105C	1.9
2	B	180	6.3	10	6	45	125C	2.8
3	C	150	6.3	15	6	94.5	105C	1.9
4	D	100	6.3	15	6	63	105C	1.9
5	B	33	10	18	6	13	125C	2
6	B	15	25	40	6	15	125C	2
7	B	15	35	40	6	53	125C	2.8

Results of external visual examination, radiography, and cross-sectioning are presented below for each part type used in this study. The parts were selected after 2000 hours of high temperature storage at 150 °C (HTS150), so some cracking in conductive polymers observed during cross-sectioning is a result of materials' degradation caused by environmental stresses.

In all cases, the major element of the capacitors is the anode aluminum plate with etched pores that have been oxidized by an anodic electrolysis process resulting in thin (dozens of nanometers) Al2O3 dielectric layers. A conductive polymer film is deposited over the aluminum oxide dielectric to form a cathode layer. A carbon layer is used to separate silver paint from the conductive polymer. The assembly is attached to the lead-frame with a silver epoxy and encapsulated with an epoxy molding compound. After that, the terminals are coated with solder and formed.

Different types of capacitors vary by the process of stacking and anode contact formation, and by the shape of the lead-frame.

Group 1. 120 µF 6.3 V

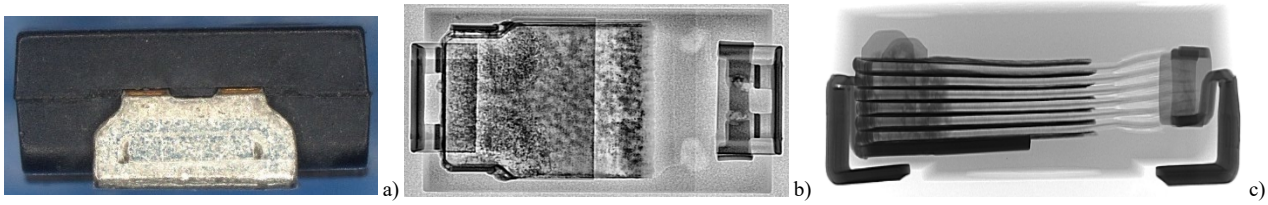

Fig.B.1.1. External visual and X-ray views of the part. Note the presence of exposed copper lead frame at the terminal's bending (a) and U-shape bending of the lead frame at the cathode terminal.

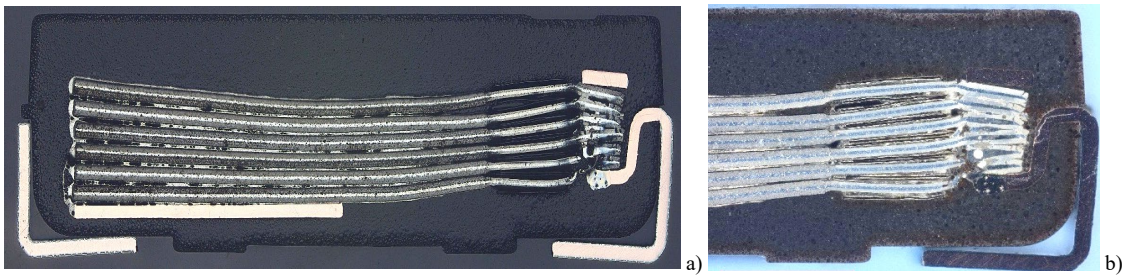

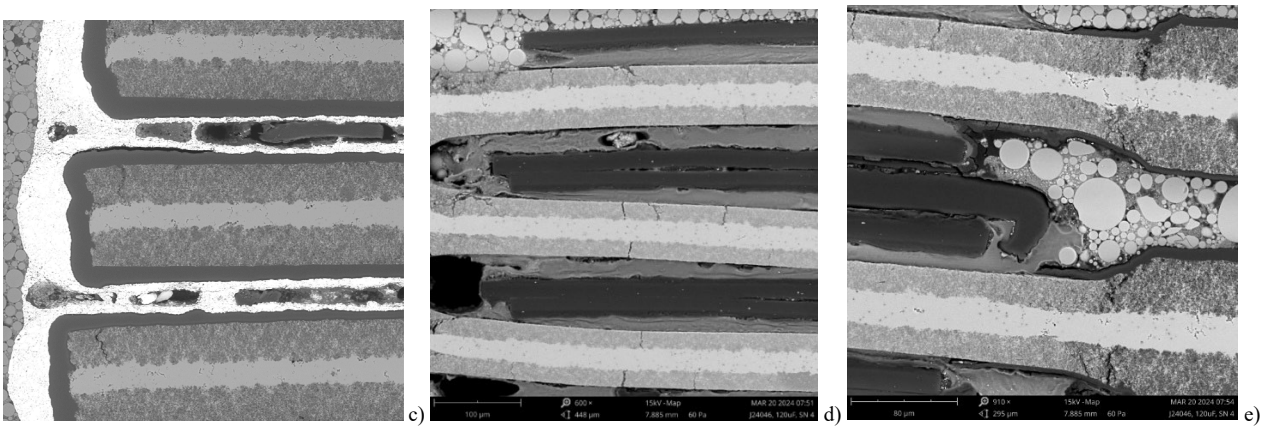

Fig.B.1.2. Optical (a, b) and SEM (c, d) views of the part after cross-sectioning along terminals. Anode contact is formed by squeezing and welding of aluminum plates at the anode end. The thickness of Al foil (with pores) is 112 and it is reduced to 67 mm before anode contact. The reason for this reduction is not clear. It is possible that it is necessary to separate anode from conductive polymer on the top of cathode area with insulating silicone. The thickness reduction area has a greater risk of cracking in Al plates (e).

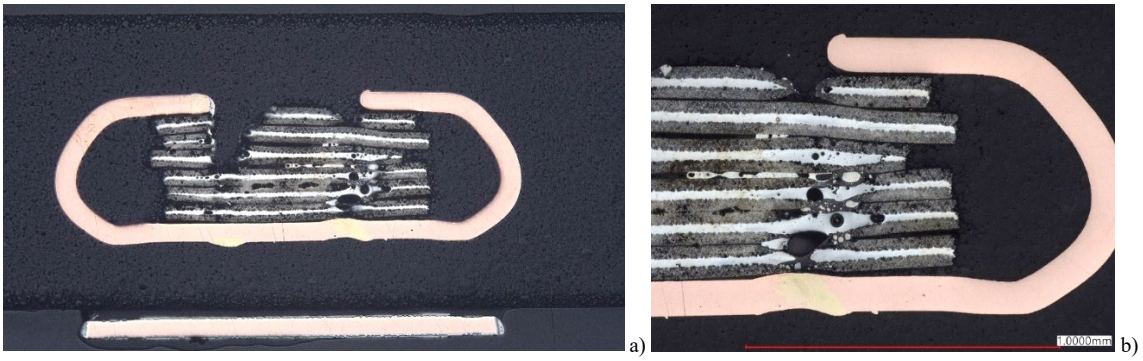

Fig.B.1.3. overall (a) and close-up (b) views of the cross-sectioning across the anode contact.

Group 2. 180uF 6.3V

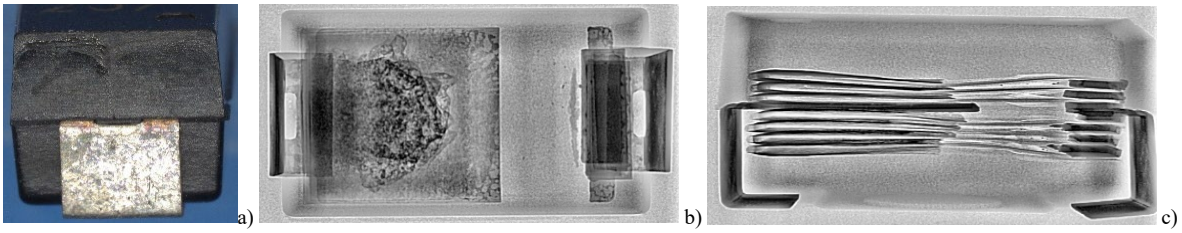

Fig.B.2.1. External visual (a) and X-ray views of the part (b, c). Note the presence of exposed copper lead frame at the terminal's bending (a).

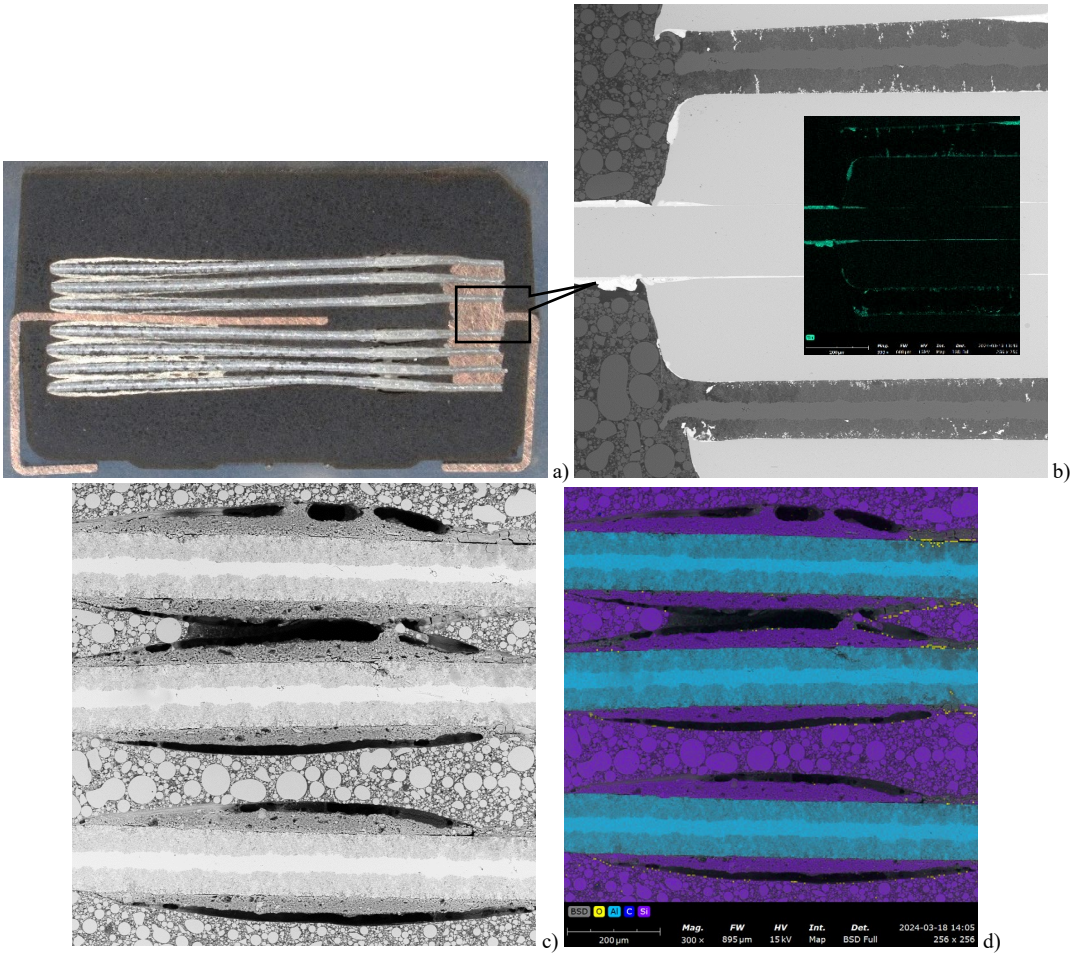

Fig.B.2.2. Optical (a) and SEM (b, c) views of the cross-sectioning. Note the use of copper spacer in the anode construction. The inset in Fig (b) shows distribution of tin used as a spacer finishing inside cracks formed during compression and welding of anode contact. Figure (d) is an EDS mapping of materials used at Al plates close to the anode contact and indicating the presence of insulating silicone. The thickness of Al plates with pores is 120 um and the thickness of aluminum is 27 um.

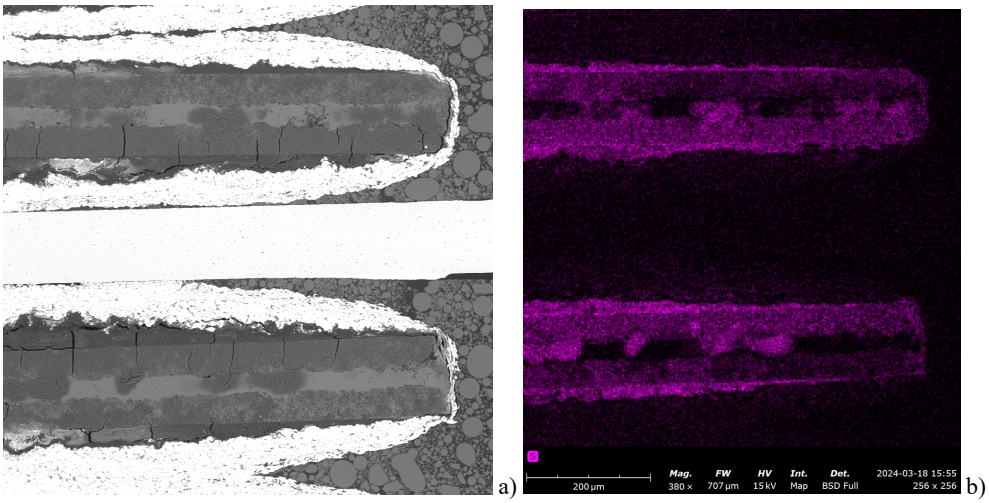

Fig.B.2.2. A SEM view (a) and distribution of sulfur (b) indicating the presence of a liquid component in the conductive polymer used.

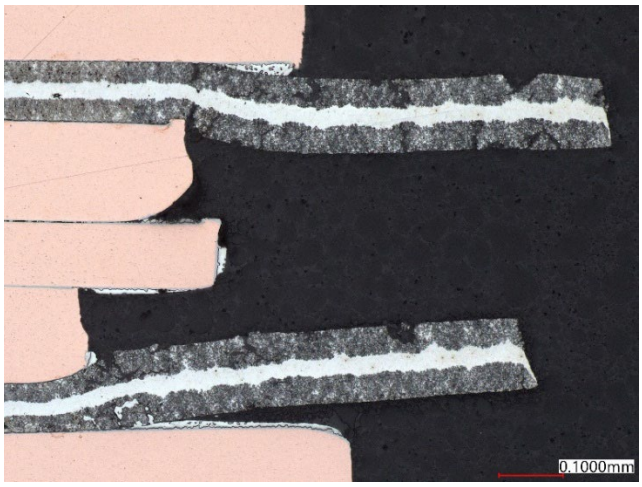

Fig.B.2.3. An optical view of the cross-sectioning across the anode contact. In this case, cracks at the burrs in spacers are not critical.

Group 3. 150uF 6.3V

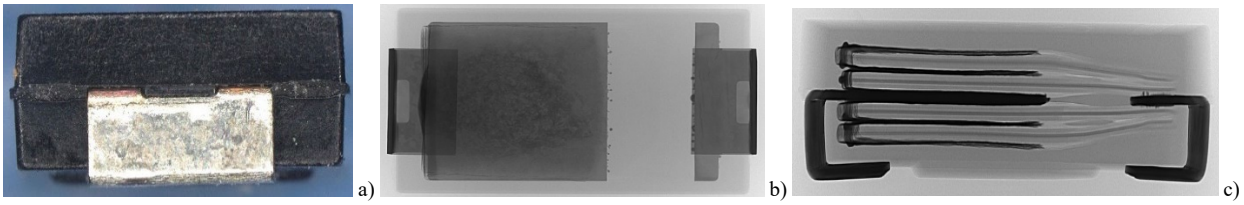

Fig.B.3.1. External visual (a) and X-ray views of the part (b, c). Note the presence of exposed copper lead frame at the terminal's bending (a).

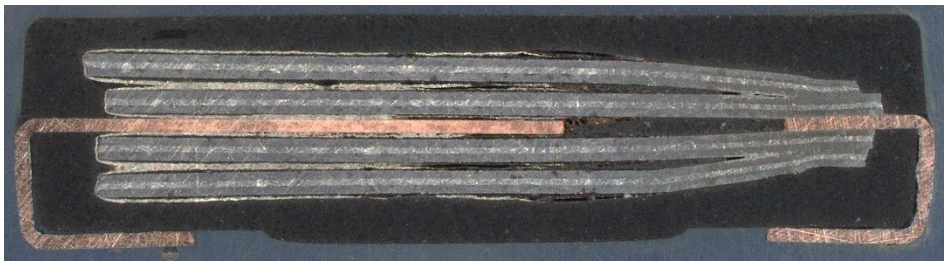

Fig.B.3.2. Cross-section of the part. EDS analyaia indicated that the lead frame was made of Cu/Ni alloy with tin finishing.

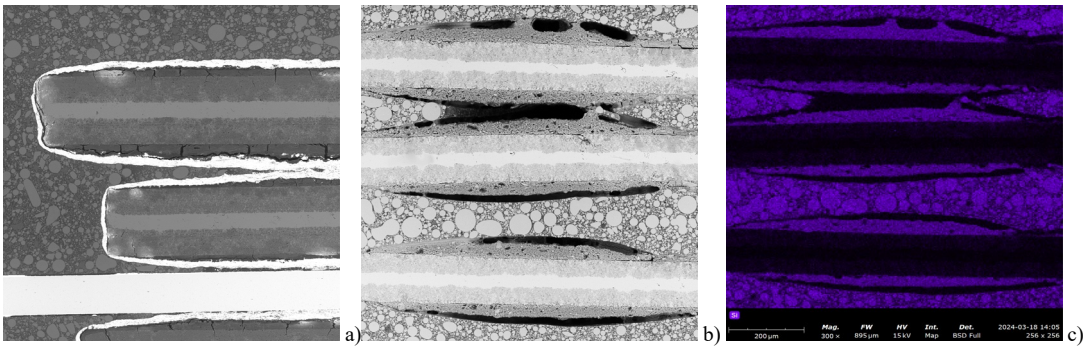

Fig.B.3.3. SEM views of the cathode end (a) and near-anode (b) areas of the cross-section. Fig (c) is an EDS mapping of materials used at Al plates close to the anode contact (b) that indicates the presence of insulating silicone.

Group 4. 100uF 6.3V

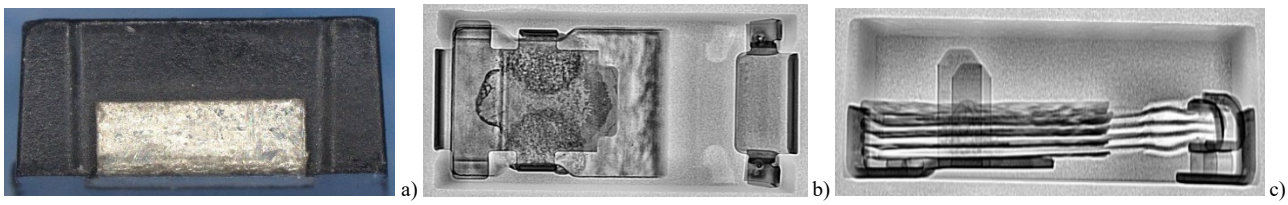

a) b) c)

Fig.B.4.1. External visual (a) and X-ray views of the part (b, c). Note the presence of exposed copper lead frame at the terminal's bending (a). Similar to 120 uF capacitors (gr.1), these parts had also U-shape bending of the lead frame at the cathode terminal (similar to group 1 capacitors).

a) b) c)

Fig.B.4.2. Overall optical views of cross-sections along terminals (a, b) and close-up of the anode welding (c).

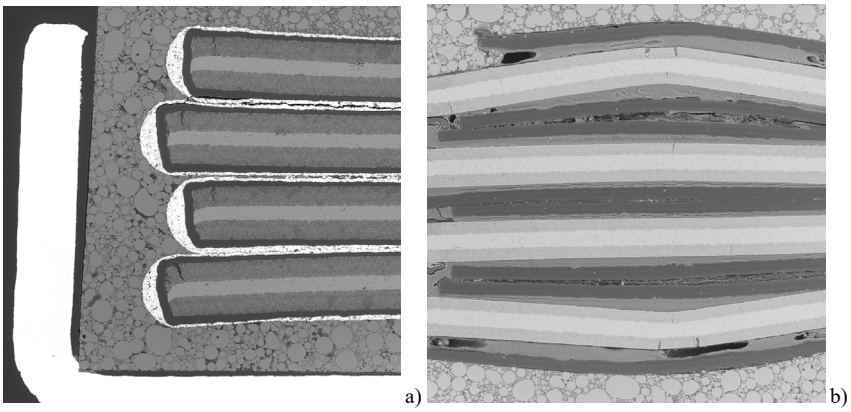

a) b)

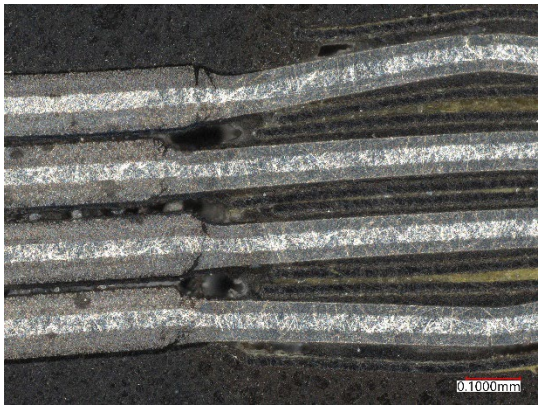

c)

Fig.B.4.3. A cathode (a) and near-anode (b) SEM and optical (c) views of the cross-section. Aluminum foil has thinning of the near-anode area that has silicone coating tom prevent shorting between conductive polymer and anode. The anode foil has multiple cracking areas.

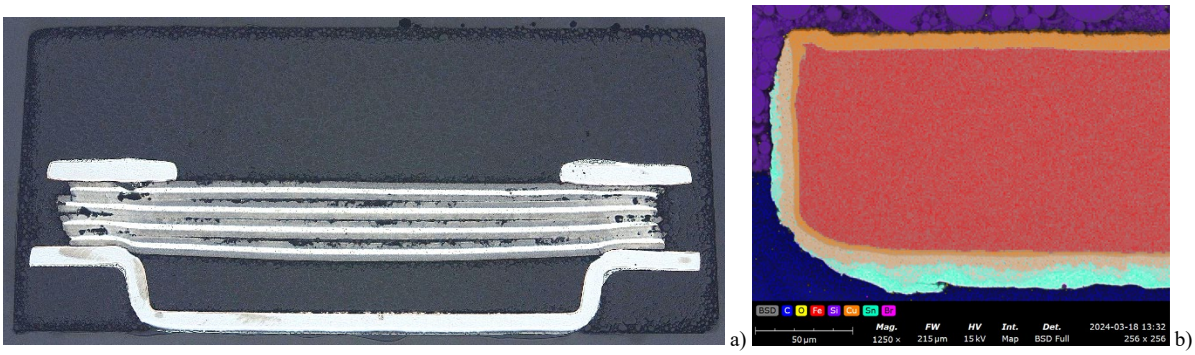

Fig.B4.4. Cross-sectioning across the anode contact (a) and EDS image of the end of the lead frame. Note that the lead frame is made of Fe/Ni alloy plated with copper and tin.

Group. 5. 33uF 10V

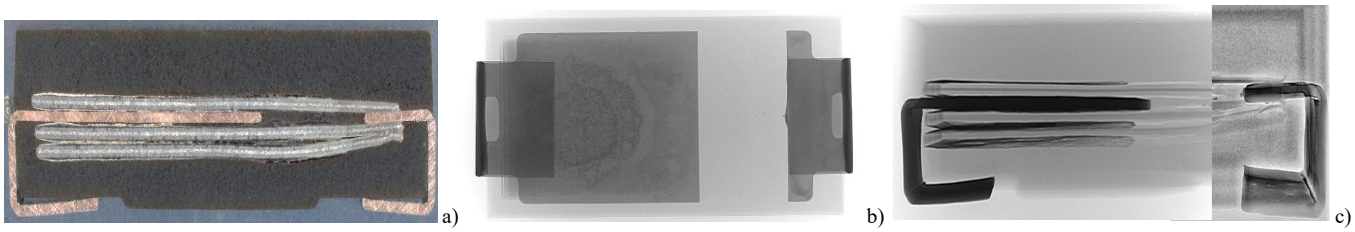

Fig.B.5.1. An optical view of the cross-section (a) and X-ray views of the part (b, c). Note that design of these parts is similar to gr. 5 capacitors. Note that the lead frame is made of a copper alloy plated with tin.

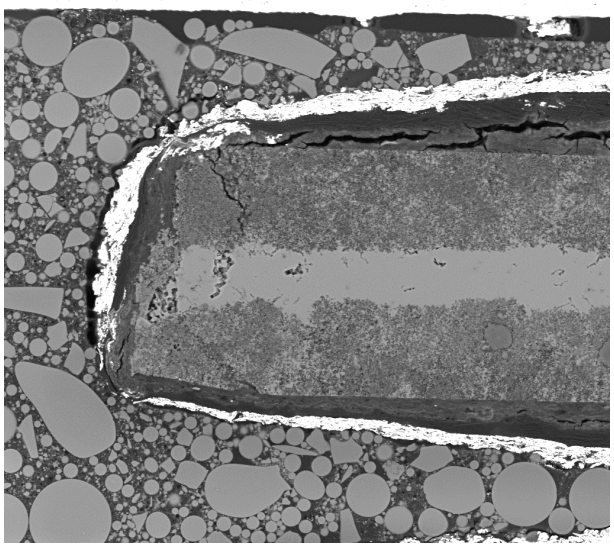

Fig.B.5.2. A SEM view of the cathode end cross-section. Cracks in the conductive polymer are due to high temperature storage of the part, but cracks in aluminum foil were likely formed during cutting of the foil.

Group 6. 15uF 25V

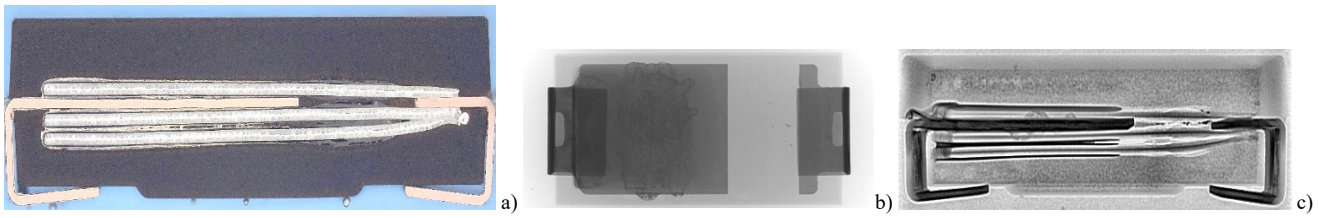

a) b) c)

Fig.B.6.1. An optical view of the cross-section (a) and X-ray views of the part (b, c). Note that design of these parts is similar to gr. 5 capacitors.

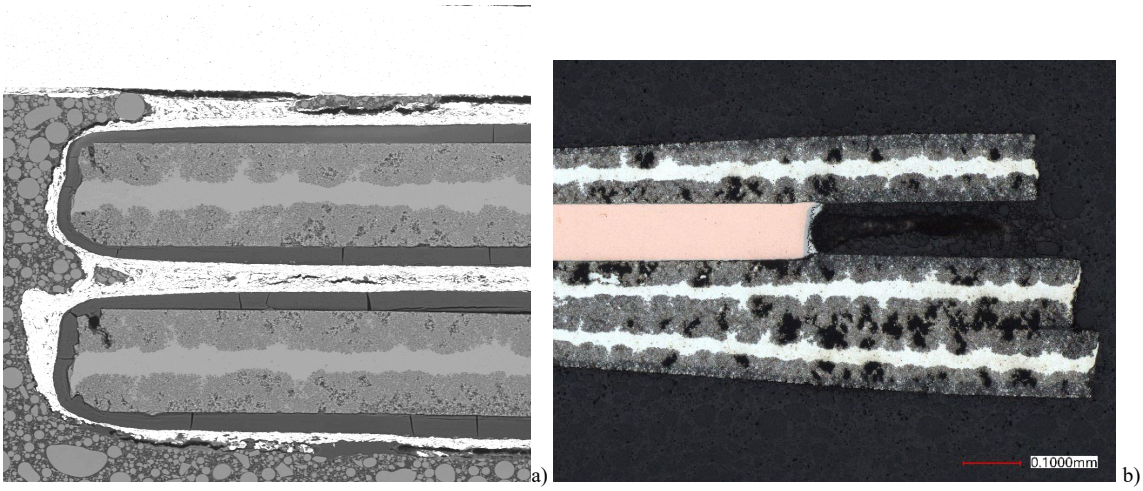

a) b)

Fig.B.6.2. A SEM view of the cathode end (a) and an optical view of the across anode cross-section (b).

Group 7. 15uF 35V

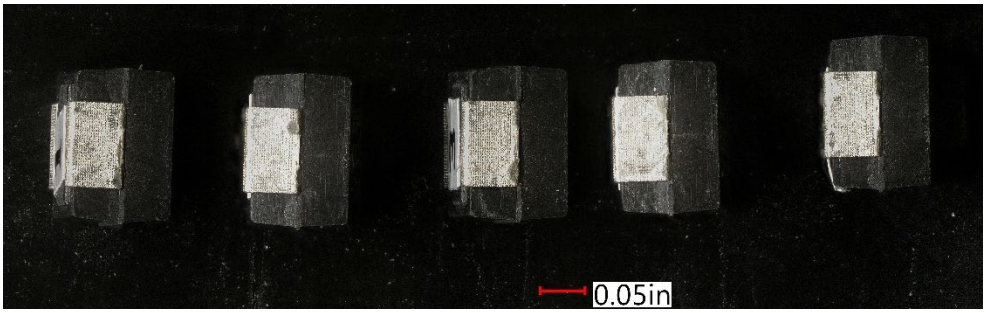

Fig.B.7.1. Optical views of terminals showing no anomalies.

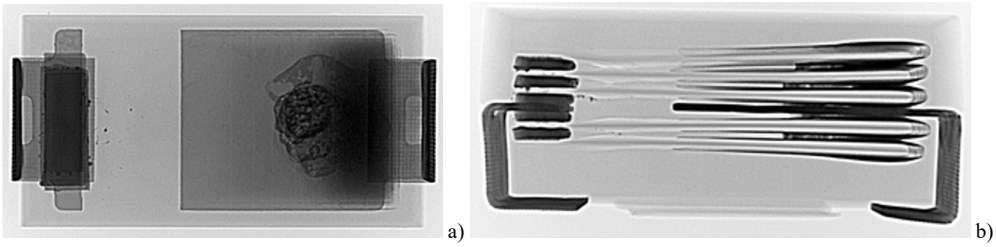

a) b)

Fig.B.7.2. Top (a) and side (b) X-ray views of the part.

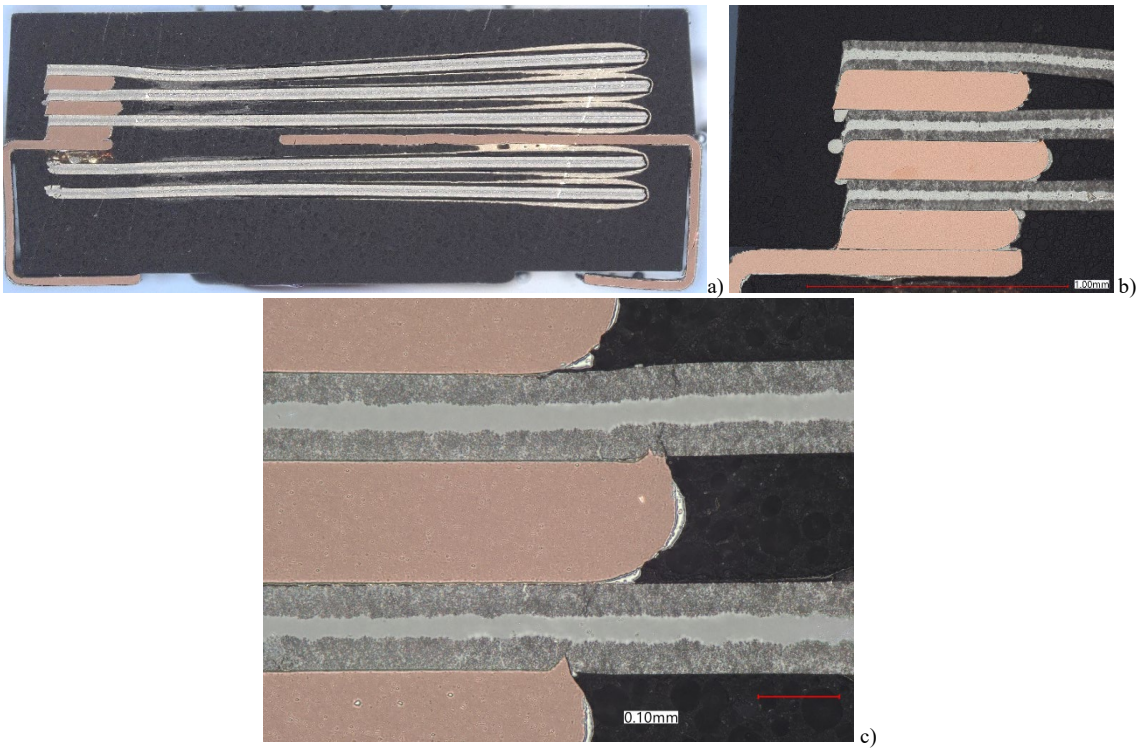

Fig. B.7.3. Cross-sectioning overall (a) and close-up of the anode area (b, c) views of the part showing copper alloy anode spacers plated with tin and cracking at the burrs in the spacers (c).

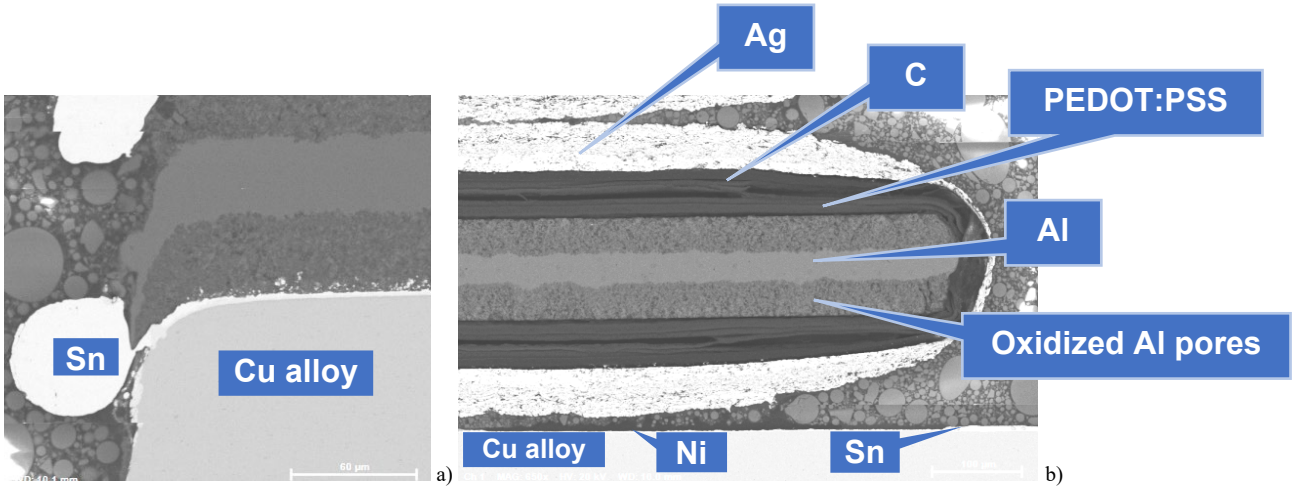

Fig.B.7.4. SEM views of the anode area shown in Fig.B.7.3.c (a) and the end of the aluminum cathode foil with surrounding materials (b). Note that the thickness of aluminum foil is 115 um. Delamination between conductive polymer layers is also typical for tantalum polymer capacitors.